MARINE HETEROTROPHIC BACTERIAL CHEMOTAXIS TO PHAGE-INFECTED *SYNECHOCOCCUS*

BY

JONATHAN MOON

A Thesis Submitted to the Graduate Faculty of

WAKE FOREST UNIVERSITY GRADUATE SCHOOL OF ARTS AND SCIENCES

in Partial Fulfillment of the Requirements

for the Degree of

MASTER OF SCIENCE

Biology

May 2023

Winston-Salem, NC

Approved By:

Sheri Floge, Ph.D., Advisor

Glen Marrs, Ph.D., Chair

Regina Cordy, Ph.D.

ACKNOWLEDGEMENTS

I would like to thank my advisor, Dr. Sheri Floge, for the opportunity to work on this project and pursue my Master's degree. I would also like to thank the Wake Forest Department of Biology and my graduate advisory committee members, Dr. Regina Cordy and Dr. Glen Marrs, for their time and investment in my studies. Thanks to our collaborators from Tufts University: Dr. Jeffrey Guasto, Dr. Richard Henshaw, and Dr. Michael Stehnach for their guidance on the project's microfluidic and computational components. Thank you also to the Northen Lab at UC Berkeley for their work on the metabolomics side of the project.

Lastly, I am very grateful to my family for their continued love and support wherever life takes me. To my wonderful fiancé, Brandi: we have been through so much together and I consider myself exceptionally lucky to call you my best friend. Thank you for being there with me through thick and thin. You are my ride or die and I cannot wait to start our next adventure together!

TABLE OF CONTENTS

LIST OF FIGURES AND TABLES

LIST OF ABBREVIATIONS

AMG ..... Auxiliary Metabolic Gene

ASW ..... Artificial Seawater

BCP ..... Biological Carbon Pump

BSA ..... Bovine Serum Albumin

CCW ..... Counterclockwise

CW ..... Clockwise

DOM ..... Dissolved Organic Matter

ESI ..... Electrospray Ionization

FDR ..... False Discovery Rate

FP ..... Fecal Pellet

FPS ..... Frames Per Second

HPI ..... Hours Post-Infection

MCP ..... Methyl Accepting Chemotaxis Protein

MS ..... Mass Spectrometry

MTA ..... Methylthioadenosine

NPP ..... Net Primary Production

PFU ..... Plaque Forming Units

PP ..... Primary Production

PS ..... Photosynthesis

SD ..... Standard Deviation

SE ..... Standard Error

TEP ..... Transparent Exopolymer Particle

ABSTRACT

Synechococcus are an important genus of marine cyanobacteria that are estimated to be responsible for approximately one-fifth of oceanic net primary production. Cyanophages are viruses that infect *Synechococcus* and can alter host gene expression and metabolite exudation prior to and following phage-induced cell lysis. Heterotrophic microorganisms can detect and navigate towards exuded metabolites, which can serve as nutrient sources, through chemotaxis. Thus, marine viruses potentially manipulate microbial interactions with infected hosts which has implications on nutrient exchange and carbon flux. Despite their high abundance and estimated impact on microbial populations, mechanisms of viral influence on the marine ecosystem are not well characterized. Additionally, no published studies have quantified bacterial chemotaxis in response to cyanophage-infected *Synechococcus* or their exudates. In this study, we utilized microfluidics and video microscopy to investigate the chemotactic responses of the marine heterotrophic chemotactic bacterium *Pseudoalteromonas haloplanktis* to *Synechococcus* exudates collected from phage-infected cultures. We also investigated chemotaxis of another marine bacterium, *Vibrio alginolyticus,* to intact phage-infected *Synechococcus*. These data build on previous work and provide new evidence to suggest that cyanophages may indeed influence microbial interactions which has the potential to impact our understanding of factors affecting nutrient and carbon flux in the marine environment.

CH I: BACTERIAL CHEMOTAXIS TO CYANOVIROCELL EXUDATES

INTRODUCTION

Approximately half of all primary production (PP) on Earth is carried out by microbial organisms in the oceans through the process of photosynthesis (PS) (1). In simplest terms, PP is the conversion of inorganic carbon sources, such as carbon dioxide (CO_2), into organic carbon compounds, such as glucose, that can be assimilated by heterotrophic organisms. Total oceanic net primary production (NPP), the total bioavailable carbon fixed by PS, is estimated to be 50Pg ($50x10^{15}$ g) per year (1,2). Photosynthetic organisms in the ocean comprise ~20% of total marine biomass of which photosynthetic bacteria (cyanobacteria) account for ~20% (3). *Synechococcus* spp. are a genus of cyanobacteria that are among the most impactful in this process and are estimated to yield ~17% of total oceanic NPP though they account for less than 10% of picoplankton (phytoplankton <2μm) in the photic zone (upper 200m of the water column) (4). *Synechococcus* populations are widely distributed across oceans at both high and low latitudes at average annual concentrations of ~10^4 cells mL^{-1} and play a critical role in the global carbon cycle (4,5). Additionally, modeling suggests future increases in the total abundances of *Synechococcus* and other cyanobacterial populations due to proliferation in existing niches and geographic range expansion as a result of increasing global temperatures (4). This contrasts with expectations for other phytoplankton species that are less well adapted to oligotrophic, nutrient poor, conditions where *Synechococcus* often thrive. Increasing surface water temperatures, as a result of global warming, contribute to stratification of the water column and reduces vertical mixing of nutrients that sink out of the upper layer (6,7). Larger phytoplankton are less well adapted to oligotrophic waters

and populations are projected to suffer in response (6,7). Thus, *Synechococcus* are expected to have an increasing importance in global carbon cycling (4), In addition to their role in oceanic PP, the *Tara Oceans* expeditionary cruises (8) indicated an association between *Synechococcus* and their viral predators with carbon export to depths of 150m based on metagenomic analyses and particle size distributions and concentrations (5). Carbon export and sequestration within the ocean's interior is an important process in the regulation of atmospheric CO_2 cycling and is facilitated through a mechanism known as the biological carbon pump (BCP) (Figure 1) (5,9). The BCP serves a critical function in the maintenance of global climatological homeostasis and is responsible for the sequestration of up to 16Gt ($16x10^9$ tons) of carbon annually (2,10). Increasing anthropogenic CO_2 emissions continues to drive the need to improve predictive carbon cycling models with respect to important primary producers such as *Synechococcus*.

Marine phytoplankton, such as *Synechococcus*, are critical components in the global carbon cycle because of their ability to generate usable carbon compounds from inorganic carbon sources (2,11,12). Therefore, it is important to understand factors that influence the ability of marine primary producers to carry out this essential function. Marine viruses are one type of pressure that *Synechococcus*, and other marine microbes, face. Viruses are highly abundant in the oceans and have been reported to reach concentrations of 10^8 viruses mL^{-1} of seawater (10). Estimates of total daily microbial mortality due to viruses range from 20-40% which implies considerable viral control over marine microbial populations (13,14). Evidence suggests an integral role of marine viruses in modulating nutrient flux within microbial communities (15–18), but their contribution to the global carbon cycle has been difficult to model due to the complexity of marine

ecosystems (19,20). Viruses are thought to influence the BCP through the proposed mechanisms of the viral shuttle and viral shunt (13). The viral shuttle enhances the efficiency of the BCP by increasing the ratio of carbon to nitrogen and phosphorous exported from the surface to deeper waters (15,21,22). Viruses have increased nitrogen and phosphorous demands due to their structural nature which can impact dissolved concentrations of these nutrients (23). Additionally, virally-infected cells have been shown to produce transparent exopolymer particles (TEP) which can facilitate cellular aggregations that sink more readily (24,25) resulting in enhanced carbon sequestration (16,26). Other evidence shows that infected cells can experience higher grazing pressure by predatory protists (27) and copepods (28) which could promote upward trophic transfer of nutrients. However, if infected cells were grazed on more frequently, they would be selectively packaged into fecal pellets (FP) which contain higher carbon to nitrogen ratios (29) and would sink at higher rates due to FP density thereby enhancing carbon export. The viral shunt (14) proposes that viral-induced lysis results in rapid release of intracellular contents, including dissolved organic matter (DOM). Viral lysis also converts particulate organic matter (POM) from live to dead states (13) and is more likely to sink compared to DOM due to its larger size of $\geq 0.2\mu m$ (14,30). DOM consists of carbon, nitrogen, and phosphorous containing compounds (18,31) and includes nutrients such as amino acids (17) and dimethyl sulfide (DMS), a climatologically relevant gas (32–34). Labile forms of DOM that remain suspended in productive waters may be recycled through the microbial loop which redirects them away from higher trophic levels and promotes microbial respiration (14,18,35). Viral-induced lysis can also release recalcitrant compounds that are less readily degraded and ultimately can be sequestered in oceans (30).

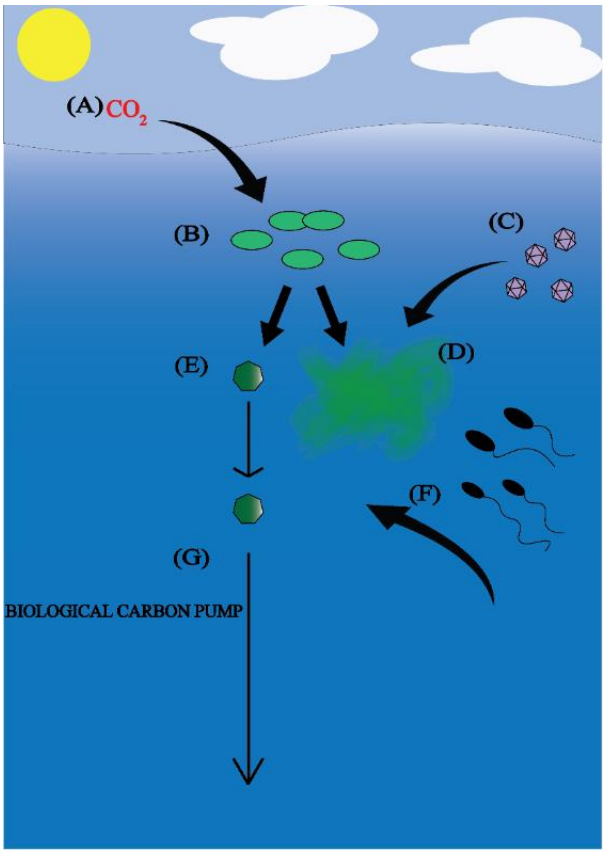

Figure 1 - The Biological Carbon Pump (BCP) (30). Simplified cartoon of the BCP adapted from Zhang et al. 2018. Dissolved inorganic carbon ($CO_{2(aq)}$ and HCO_3^-) (36) is taken up by photoautotrophs for use in PS (A & B). Phytoplankton constitutively release labile DOM that can be utilized by heterotrophs. Viruses may disrupt the transfer of nutrients from primary to secondary producers through the 'shunt and pump' (C) (13) via cell lysis which creates ephemeral nutrient zones (D) and simultaneously increases the ratio of carbon to nitrogen and phosphorous export in the form cell debris and POM (E). Labile organic matter is detected and assimilated by chemotactic heterotrophic microbes (F). Recalcitrant, carbon rich organic matter sinks at faster rates (G) which can sequester carbon in the deep ocean for up to millennia.

Cyanophages are a specific group of viruses that only infect cyanobacterial hosts. The cyanomyovirus family of cyanophages are often found to infect *Synechococcus* (37–39) and have been classified as T4-like double stranded DNA viruses (40). Cyanomyoviruses exhibit morphological similarities to the *E. coli* T4 phage and are constructed of an icosahedral capsid protein that stores the phage genome, a contractile sheath through which the phage genome is injected into the host, and tail fiber proteins that mediate phage attachment (41). Although specific host receptors for cyanophage attachment are not well described, it has been suggested that the cyanobacterial lipopolysaccharide may facilitate this process (42). Auxiliary metabolic genes (AMG) encoded by cyanophages are homologs of host genes that may promote important host cell functions and ultimately facilitate enhanced cyanophage reproduction (43–45). Manipulation of host cell processes during infection can alter the composition of host-derived metabolic exudates which can affect microbial population dynamics and interactions (16,17,33,46).

Marine heterotrophic microorganisms acquire and assimilate organic carbon compounds exuded by phytoplankton. Large regions of the ocean are oligotrophic and heterotrophic organisms must be able to actively seek out nutrient sources (47). One mechanism of navigation utilized by motile bacteria is chemotaxis which is the ability to sense and respond to chemical stimuli through cellular locomotion. Bacteria exhibit motility through the use of one or more flagella which are composed of a multiprotein complex that acts as a molecular motor to propel the cell and is typically facilitated by proton or sodium motive forces. Methyl accepting chemotaxis proteins (MCP) bound in the bacterial cell membrane bind a myriad of chemical signals both attractive and repulsive.

MCP interaction with chemical stimuli triggers a phosphorylation cascade that ultimately activates a response regulator protein that subsequently activates the flagellar switch. This interaction initiates flagellar rotational switch from counterclockwise (CCW) to clockwise (CW) causing a transition in motility from a 'run' to a 'tumble' or to a 'reverse' which randomly reorients the bacterial cell. This dynamic cycle of forward swimming followed by random directional changes is known as a biased random walk (48,49) and is what allows chemotactic bacteria to navigate in response to a chemical gradient. A general schematic of the bacterial flagellum is diagramed in Figure 2.

The marine heterotrophic bacterium, *Vibrio alginolyticus*, produces a single polar flagellum in fluid media powered by Na^+ motive force (50) and was shown to exhibit a run-reverse-flick pattern of motility (51). *Pseudoalteromonas haloplanktis*, another marine heterotrophic bacterium, similarly produces a unipolar, monotrichous flagellum that facilitates a run-reverse motility dynamic (52,53). Open ocean environments are often nutrient poor and subject to turbulent mixing forces through advection and oceanic currents. Low nutrient concentrations in addition to continuous displacement due to physical forces and Brownian motion are thought to select for organisms that can rapidly detect and respond to nutrient sources. To this end, both *V. alginolyticus* and *P. haloplanktis* have been shown to be capable of swimming at speeds exceeding 100μm s^{-1} in response to chemical gradients and in the presence of phytoplankton (52–55).

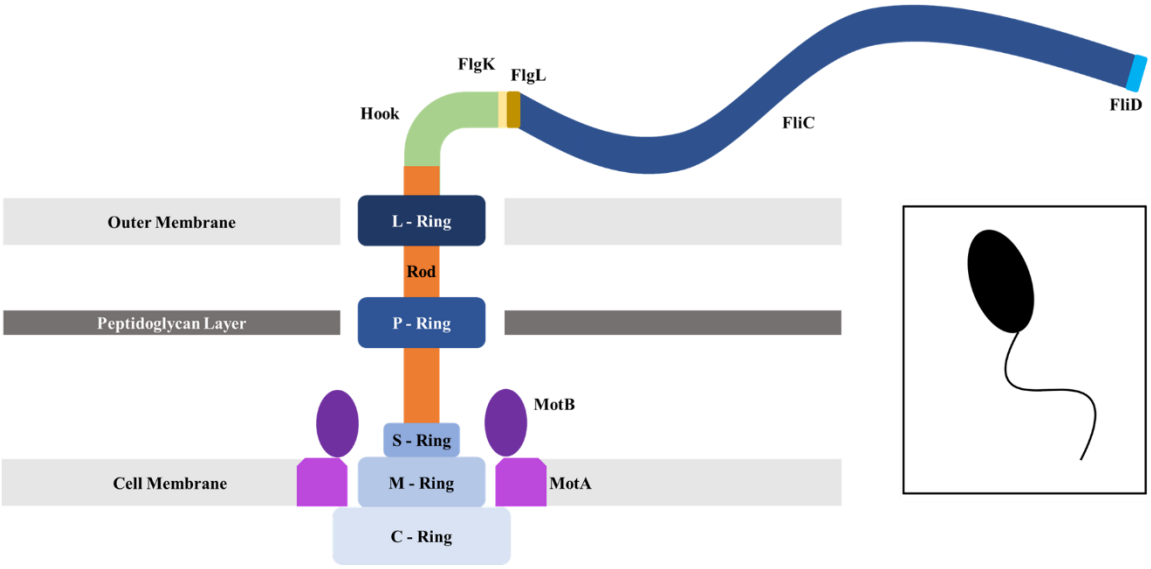

Figure 2 - The Bacterial Flagellum. The general flagellar structure is pictured on the left. A cartoon of a polar, monotrichously flagellated bacterium (e.g., *V. alginolyticus*) is pictured inside the boxed area to the right. The flagellum filament itself is a multi-subunit structure made of FliC monomers. This filament is attached to the hook protein through hook associated proteins. A multi-protein complex anchored in the cell membrane spans the peptidoglycan layer and outer membrane and controls the rotational direction of the flagellum. When the flagellum rotates CCW, the cell 'runs' in a forward motion. A change to CW rotation results in a 'reverse' of motility in *V. alginolyticus* that then results in a 'flick' upon a switch back to CCW rotation which may turn the cell ~90° before re-initiating a 'run' (51,56).

Exudates released by marine phytoplankton represent important nutrient sources for heterotrophic bacteria. Acquisition and assimilation of dissolved organic carbon compounds produced by phytoplankton can stimulate the growth of heterotrophic microbial populations and is a route by which organic carbon compounds can be exchanged (35,57). Bacterial cells adjust gene expression and protein translation in response to environmental stimuli on temporal scales of minutes (58–60) which may expeditiously affect their ability to utilize specific metabolites. Phages also modulate and reprogram host gene expression during infection to promote phage replication (46,61). Phage-induced alterations in extracellular metabolite concentrations could potentially affect chemotactic responses of heterotrophic bacteria during infection due to changes in chemical gradients encountered by chemotactic cells. Bacterial chemotaxis to phytoplankton exudates and uninfected cells has been previously explored (52,62–66). Though currently, no published data exist investigating differences in chemotactic responses to phage-infected phytoplankton or their exudates. Elucidating ecological effects of phage-infection of phytoplankton may reveal previously uncharacterized mechanisms acting on nutrient flux in the marine environment. Considering estimates of viral-induced population turnover and the geographic scale of the ocean, these data have the potential to fundamentally alter our understanding of and appreciation for the role of marine viruses on carbon and nutrient cycling.

Previous work showed that infection with the cyanophage S-SSM5 differentially altered the transcriptome and both intracellular and extracellular metabolite abundances of the host *Synechococcus* WH8102 as compared to uninfected controls (46). Extracellular metabolites that were more abundant in phage-infected cultures included nucleotides,

amino acids, and derivatives of both classes of molecules. The bacterium *V. alginolyticus* exhibited positive chemotaxis towards metabolic exudates collected from both phage-infected and uninfected *Synechococcus* WH8102 cultures (Henshaw et al., [Unpublished manuscript, in progress]). When the exudates from phage-infected and uninfected cultures were presented to *V. alginolyticus* in a competition style assay, *V. alginolyticus* responses were preferentially biased towards exudates collected from phage-infected cultures. This result demonstrated that exudates from phage-infected *Synechococcus* cultures contained either greater abundances of attractive metabolites or that certain attractive metabolites were present in the phage-infected culture exudates that were absent from uninfected cultures. The experiments conducted herein expand upon this work through quantification of the chemotactic responses of a different marine heterotrophic bacterium, *P. haloplanktis*, to the same exudate samples collected from phage-infected and uninfected *Synechococcus* WH8102 cultures. These results provide new evidence to support that the composition of metabolites exuded by phage-infected *Synechococcus* differs from uninfected cells to a degree that is detectable by chemotactic bacteria.

MATERIALS AND METHODS

Collection of Phage-Infected and Uninfected *Synechococcus* Culture Exudates

Exudates were collected from phage-infected and uninfected *Synechococcus* cultures as previously described (46). Briefly, samples were collected from both phage-infected and uninfected *Synechococcus* cultures every ~2 hours and were filtered using 0.2µm pore size PES filters. Exudate samples were flash-frozen in liquid nitrogen and subsequently stored at -80°C until their use in chemotaxis experiments. Prior to each chemotaxis experiment, exudate samples were thawed and kept on ice. Immediately before their use, exudate samples were equilibrated to room temperature.

Bacterial Growth Conditions and Media

V. alginolyticus (YM4) and *P. haloplanktis* (ATCC 700530) were grown in M2216 marine broth (Becton Dickinson, Sparks, MD #279110) which was prepared following the manufacturer's specifications. After autoclaving, media was centrifuged to pellet sediments. Bacterial cultures were grown only in media that did not contain sediments. *V. alginolyticus* were grown in a Benchmark MultiTherm incubator at 30°C with agitation at 600 RPM. *P. haloplanktis* cultures were grown at room temperature (~22°C) without agitation.

Preparation of Bacterial Suspensions

V. alginolyticus were grown in M2216 marine broth overnight for ~18 hours. The following day, subcultures were prepared at a dilution of 1:100 in fresh M2216 broth. Subcultures were grown for 3 hours at 30°C with 600 RPM agitation. Cultures were then centrifuged at 1,500xg for 5 minutes at 20°C. The supernatant was removed and the cell pellet was washed in artificial seawater (ASW) (67,68) by tap mixing to gently re-suspend

cells. The washed suspension was centrifuged again and the final cell pellet was gently re-suspended in a volume of 500μL ASW to a concentration of ~10^9 cells mL^{-1}.

P. haloplanktis were grown in M2216 marine broth overnight for ~24 hours at room temperature without agitation. Cell cultures were centrifuged at 1,500xg for 5 minutes to pellet cells. The supernatant was removed and the cell pellet was washed in ASW by tap mixing to gently re-suspend cells. The washed suspension was centrifuged again and the final pellet was gently re-suspended in 200μL ASW to a concentration of ~10^9 cells mL^{-1}.

Chemotaxis and Microfluidics Experiments

Microfluidic channels were constructed from polydimethylsiloxane (PDMS, Sylgard 184) using soft lithography (69). The channel design consists of three inlets with a single outlet allowing for influx of multiple fluids containing different components. The PDMS chip was plasma bonded to a standard microscope slide (25mm x 75mm x 1mm) to allow for imaging of cells within the channel. The microfluidic device (Figure 3) was first primed with 0.5% BSA (Sigma-Aldrich, St. Louis, MO #A7906) in Milli-Q water for 30 minutes to act as a surfactant and reduce bacterial adhesion to the device. Prior to creating the cell suspensions, two 1mL and one 0.25mL Hamilton gas tight syringes (Hamilton, Reno, NV #81301, #81101) were fitted with 22-gauge Leur lock needles (Fisher Scientific, Pittsburgh, PA #K868280-2201) with Tygon tubing of 0.020in. inner diameter and 0.060in. outer diameter (Fisher Scientific, Pittsburgh, PA #NC0578437) attached. Each syringe was pre-loaded with ASW to purge air from the system. Cell (0.25mL), chemical (1mL), and ASW (1mL) suspensions were loaded into individual syringes whilst maintaining the gas tight state of each device. 200μM L-serine (Sigma-Aldrich, St. Louis, MO #S4500) and 200μM phenol (Sigma-Aldrich, St. Louis, MO #P1037) were loaded into chemical syringes

in separate chemotaxis validation experiments. The loaded syringes were then connected to the microfluidic device via the Tygon tubing, again ensuring that no air entered the system. Fluid components were always injected into the device at the same physical injection port as diagrammed (Figure 3A).

A mechanized syringe pump (Harvard Apparatus Ph.D. Ultra) was employed to exert uniform control of the flow rate of each syringe and a Zeiss AxioObserver inverted microscope was used to visualize cells within the microfluidic device (Figure 3C). A 10x objective (0.25NA) was used to observe the channel and images were collected using a FLIR Blackfly S camera (Teledyne FLIR, Wilsonville, OR #BFS-U3-51S5M-C) at a frame rate of 1 frame per second (FPS) for 600 seconds (10 minutes). The camera adapter included an additional 0.63x magnification which resulted in a final magnification of 6.3x.

To establish gradients within the microfluidic device, the syringe pump was operated at a flow rate of 25μL min^{-1} for 5 minutes. After this 5-minute period, the flow was stopped and the outlet tubing was simultaneously clamped to seal off the system. Image capture commenced immediately following flow stoppage. Three replicate experiments using independent bacterial cultures were performed for each condition. Each replicate experiment consisted of three individual 10-minute runs and the data from the three runs were averaged to yield the final output for each biological experimental replicate.

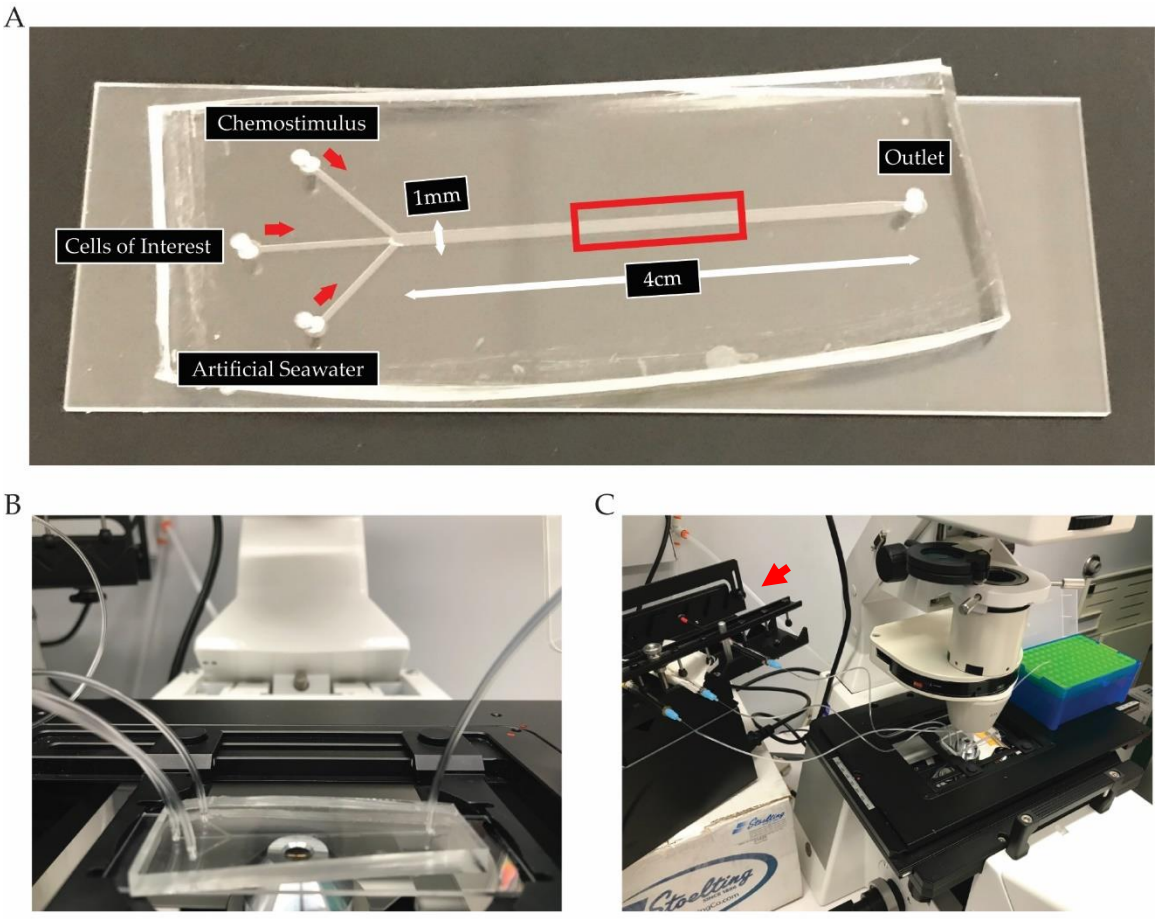

Figure 3 – Microfluidic Device and Set Up. (A) The microfluidic chambers were cast in polydimethylsiloxane (PDMS) and were designed with three injection ports and a single outlet allowing three different solutions to be flowed into the channel simultaneously. (B) Microfluidic channel set up on the inverted microscope with tubing connected to solution containing syringes. (C) Uniform fluid flow rate was controlled using a mechanical syringe pump (red arrow) that allowed for consistent establishment of fluid gradients within the channel.

Image Analysis

Three MATLAB scripts were used to identify cells in each image: 'bpass', 'pkfnd', and 'cntrd' (70). First, each image within the timelapse image sequence is smoothed with gaussian blur and undergoes a bandpass filter to reduce noise. The filtered images are then passed to 'pkfnd' which uses the 8-bit pixel values as a measure of intensity and corresponds to particle (cell) locations within the image. 'pkfnd' identifies particles at pixel level accuracy and the images with particle locations are then passed to 'cntrd' which further accurizes identifications to sub-pixel level (Figure 4). Custom MATLAB code was then used to calculate the accumulation index, β(t), at each time point from the resulting particle locations in the timelapse image series. Only particles located within a 200μm width from the left and right edges of the channel were considered in the β(t) calculation which preferentially selects for highly motile cells within the population. The β(t) value is calculated as:

$$\beta(t) = \frac{N_L(t) - N_R(t)}{N_L(T) + N_R(T)}$$

where β(t) represents the accumulation index which describes population level cell motility. A positive value indicates a net movement to the left side of the channel and is calculated by subtracting the number of cells on the right side of the channel (N_R) at each time point (t) from the number of cells on the left side of the channel (N_L) at the same time point. The difference is then divided by the sum of all particles on the left ($N_L(T)$) and right ($N_R(T)$) side of the channel at the final time point to normalize the data. β(t) is calculated for all images in the time series and plotted as cell accumulation as a function of time.

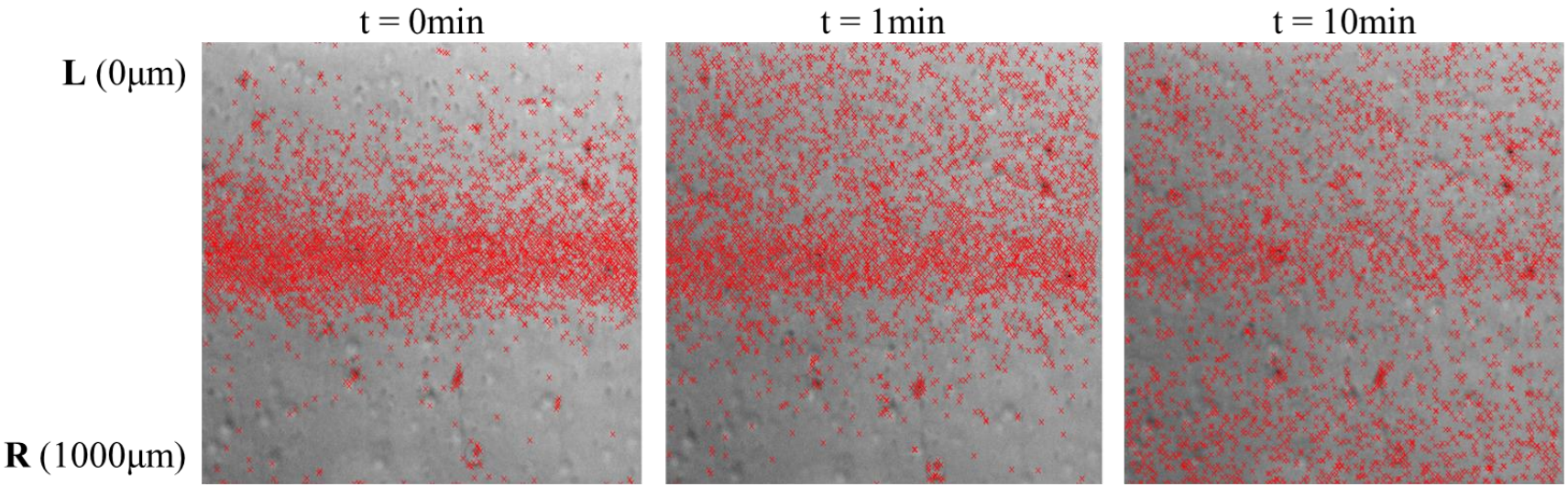

Figure 4 – Particle Detection in MATLAB. Examples of three images taken at different time points during a chemotaxis assay. The result of image processing with bpass, pkfnd, and cntrd is shown. Images are rotated 90° for visual continuity with data presented herein with the left (L) and right (R) sides of the channel noted. Each red marker indicates an individual cell location identified through thresholding input parameters. When performing timelapse analysis, a background image is created based on the total image stack composite and is subtracted from all images prior to the final output.

C18 Nonpolar Metabolomics Analysis

Metabolomics data were generated from exudate samples collected from phage-infected and uninfected *Synechococcus* WH8102 cultures using an LC-MS/MS-ORBITRAP approach as previously described (46). Samples for metabolomics analysis were collected every ~2 hours following phage addition to cultures. Exometabolites were isolated by filtering collected culture samples through a 0.22μm filter. Nonpolar analyses were performed in R by first excluding identified compounds with a minimum raw peak height $<1x10^4$. Raw data were $\log_{10}$ transformed and metabolites were considered differentially abundant at each time point if the $\log_{10}$ fold change (FC) between phage-infected treatment and uninfected control ≥ 0.1 (~25% difference) and false discovery rate (FDR) ≤ 0.05. FDR was used to control for type I error (false identification of a difference in metabolite abundance between phage-infected and control conditions) and was approximated from *t*-test comparisons with Benjamini – Hochberg correction applied to resulting *p* values. Compound identifications were made utilizing the Global Natural Products Social Molecular Networking (GNPS) database (71) in conjunction with the Cytoscape software package (72) which was incorporated to increase the ease of data visualization. The untargeted C18 mass spectrometry (MS) dataset with compound identifications determined via GNPS were used to generate a reference network in Cytoscape. Filtering of the untargeted MS dataset was then performed as described and the resulting compounds were imported as a table and matched to the reference network. Known compounds that were positively identified in GNPS based on factors including *m/z*, retention time, and precursor mass and that passed the filtering criteria were extracted from this list.

RESULTS

Validation of the Microfluidic Device

The microfluidic system and protocol were initially evaluated for technical accuracy and consistency. Initial testing was performed to evaluate fluid flows within the device over the duration of the experimental time series. Three different colored dyes, red, green, and blue, were added to three separate aliquots of Milli-Q water and were then loaded into individual gas tight syringes. Fluid flow into the microfluidic device was controlled by the mechanical syringe pump using the same settings as for biological samples. When the flow was stopped, images were taken at a rate of 1FPS for 10 minutes (Figure 5). Immediately following the termination of flow at t = 0 minutes, three individual fluid bands were observed. The colored dye within each separate fluid was distinct and clear boundaries were observed between them. Notably, the width of the central green band was compressed as compared to the left and right bands. The central fluid band is injected from a 0.25mL syringe while the left and right fluids originate from 1mL syringes. By t = 2 minutes, diffusion of fluids has begun and the central band is no longer readily distinguishable. The diffusion process occurred steadily throughout the remainder of the time series and was consistently observed over three replicate runs.

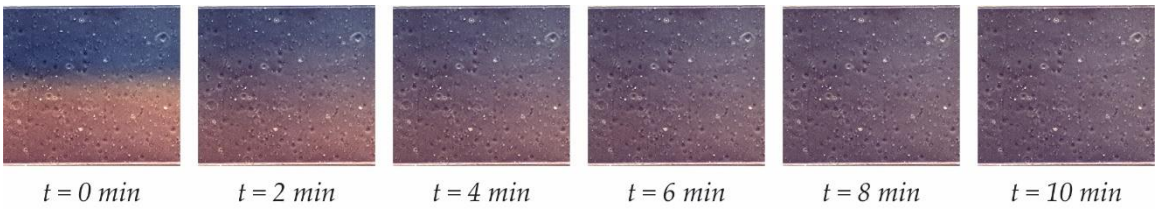

Figure 5 – Relaxation of Gradients Within the Microfluidic Device. Diffusion of colored dyes across the channel begins almost immediately following fluid flow stoppage. However, gradients between individual fluid streams persists through 6 to 8 minutes. Dyes have diffused homogenously throughout the channel by 10 minutes.

Model Chemical Compounds Provide Confirmation of Assay Viability

Three biological replicate control experiments for each model bacterial species, *V. alginolyticus* (Figure 6A) and *P. haloplanktis* (Figure 6B), were performed to further confirm proper implementation of the microfluidic technique and image analysis. Plotted lines show the mean of three biological replicates as a solid black line with the standard error (SE) shown as a color-shaded area. As expected, *V. alginolyticus* exhibited positive chemotaxis in response to a concentration of 200μM serine and was repelled by concentrations of 200μM phenol (51,73–75). We observed a strong response of *V. alginolyticus* to both stimuli immediately following introduction to the chemical gradient in all three replicate experiments. In response to 200μM serine, maximum β(t) values for each replicate were calculated as 0.92, 0.85, and 0.81 and were recorded at t = 267s, 369s, and 402s, respectively. These β(t) values indicate that 80-90% of all motile cells chemotaxed towards serine at the point of maximum accumulation in each experiment. When *V. alginolyticus* were exposed to 200μM phenol, we observed an approximately

equal and opposite maximum response (β(t) = -1.1, -0.71, and -0.67). Finally, β(t) values ranged between -0.01 to 0.28 in all three ASW control replicates and was not indicative of a strong directional motility bias. The positive accumulation that was observed in these control assays with ASW was deemed likely the result of a slight background flow within the channel that pushed the cells leftward and registered as positive accumulation.

A probability density function (PDF) was calculated for each image in the time series based on binned (n = 30 bins) cell position data across the channel (Figure 7). The PDF describes the likelihood of locating a particle within a fixed physical width within the microfluidic channel that corresponds to a specific range on the x-axis. The PDF is calculated for each time point (1FPS x 600s = 600 images) by building a histogram for each image detailing the total number of cells in each of n = 30 bins that correspond to a physical distance of ~33.95μm or 62 pixels (image width = 1860 pixels or ~1000μm). Raw position counts in each bin are normalized to PDF as defined by $v_i = c_i/N \times w_i$ where v_i = bin probability value, c_i = number of cells within a bin, N = total number of cells in all bins, and w_i = width of each bin in pixels. The center points of each bin on the x-axis are calculated and used as points to generate the PDF curve for each image which is then used to generate density plots for visualizing cell positions over time. Heat maps were generated to visualize cell positions within the channel based on PDF normalized cell densities across the time series (Figure 8).

Model compound experiments using 200μM serine, 200μM phenol, and ASW were replicated using *P. haloplanktis*. Maximum β(t) were calculated in response to 200μM serine as 1.3, 0.61, and 0.94. Overall, these responses occurred more quickly as compared to responses by *V. alginolyticus* and were recorded at t = 18s, 34s, and 162s, respectively

(*V. alginolyticus* maximum β(t) occurred at t = 267s, 369s, and 402s). Interestingly, *P. haloplanktis* were not repelled by phenol at a concentration of 200μM in all three replicates and responses remained bounded within the range of -0.26 to 0.35 for the duration of each experiment. No bias in motility was observed when *P. haloplanktis* chemotaxis was assessed in response to the no stimulus control, ASW. β(t) values in response to ASW were bounded between -0.09 and 0.22 across all replicate experiments.

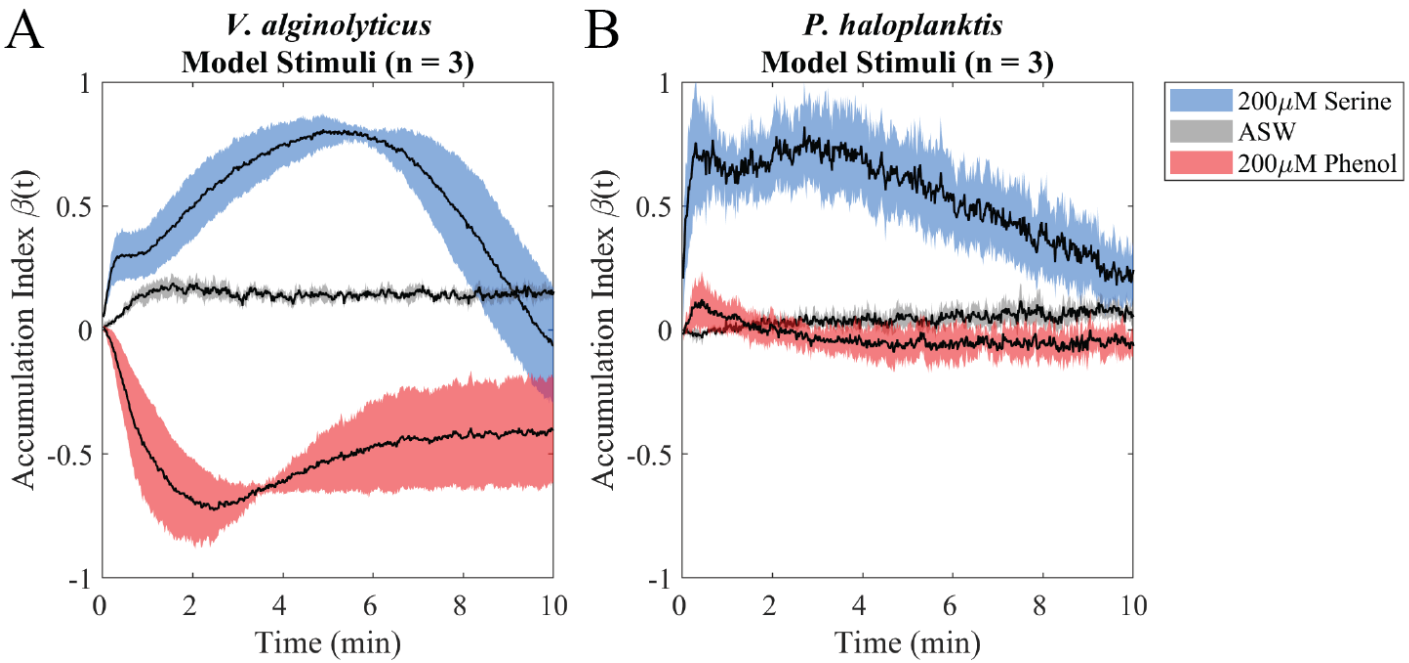

Figure 6 – Bacterial Chemotactic Responses to Model Chemical Compounds. *V. alginolyticus* (A) and *P. haloplanktis* (B) chemotaxis to the chemical attractant serine (blue), the repellent phenol (red), and ASW as a no stimulus control (grey). Each curve is plotted as a mean of three replicates with the SE of the mean shown in the color shaded region. β(t) indicates directional bias of cells within the channel in response to chemical stimuli. A positive β(t) results when cells preferentially accumulate within a 200μm width from the left edge of the channel. A negative value indicates biased cell movement to a region of 200μm from the right edge.

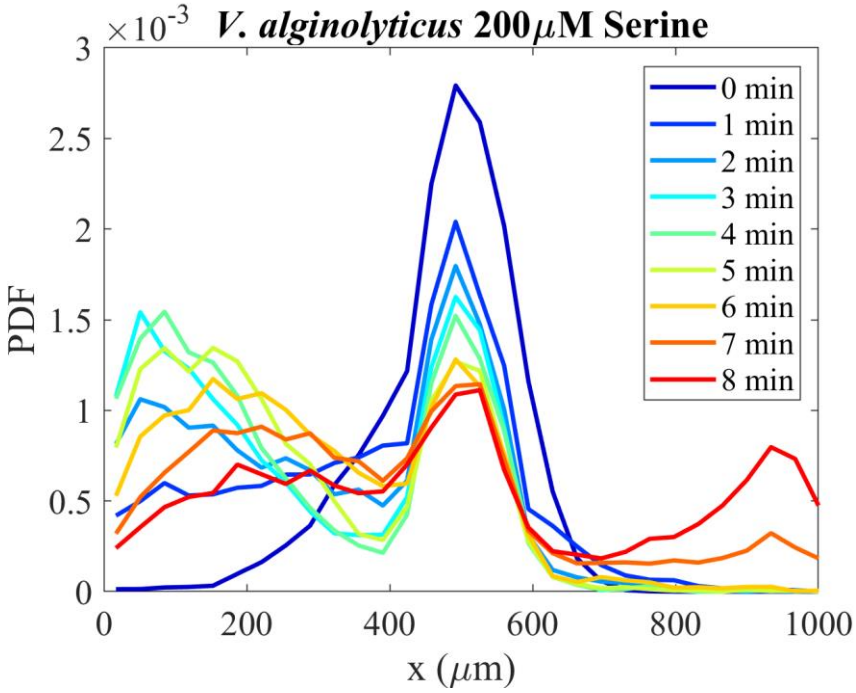

Figure 7 – Probability Density Function (PDF). PDF calculation for a single *V. alginolyticus* chemotaxis experiment in response to 200μM serine over a 10-minute time series. PDF corresponds to cell density. At 0 minutes, most cells are located within the central 200μm width of the channel between x = 400 to 600μm. As *V. alginolyticus* senses serine, they swim towards higher concentrations of serine on the left side of the channel (0 to 400μm) while the serine gradient is strongest. Peak accumulation is observed between 4 to 5 minutes following the start of the experiment. As the serine gradient relaxes and serine diffuses across the channel, *V. alginolyticus* change the direction of their motility in response as shown by an increasing PDF within the 600 to 1000μm range at later time points in conjunction with decreasing PDF on the left side of the channel.

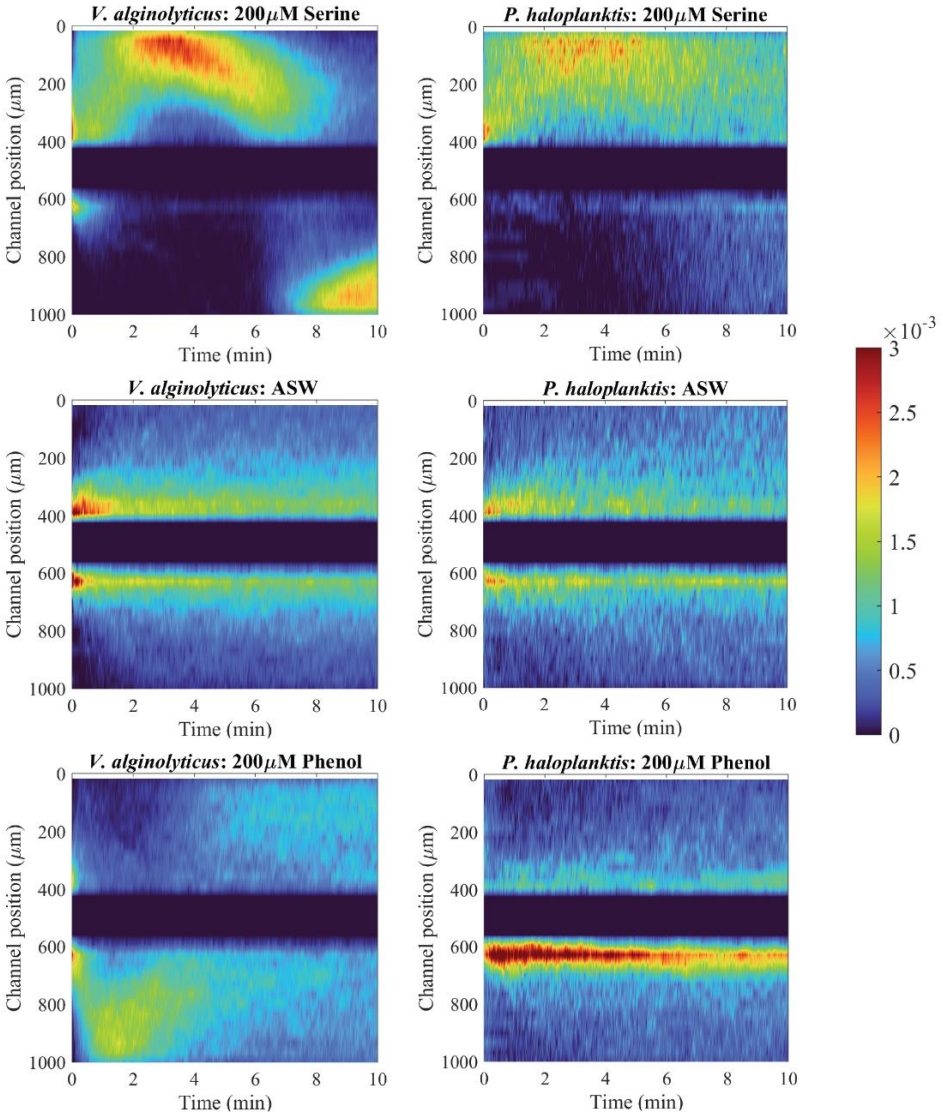

Figure 8 – Density Plots Representing Cell Localization in the Microfluidic Device. Surface (density) plots were constructed in MATLAB using individual cell location coordinates to visualize relative cell concentration and position within the channel over time. The central 200μm region containing a non-chemotactic proportion of the population was omitted to improve visualization. Scale bar represents the calculated PDF for each experiment.

P. haloplanktis Chemotaxis to Exudates from Phage-Infected *Synechococcus* Cultures

Synechococcus WH8102 culture exudates were collected in a previous infection experiment using the phage S-SSM5. Exudates from phage-infected cultures were collected at 2 hours and 12 hours post-infection (HPI) (46) and were used in chemotaxis assays to evaluate *P. haloplanktis* responses. Exudates were collected from uninfected *Synechococcus* cultures at the same time points. Three chemotaxis experiments were conducted for both control and phage-infected exudates, each using a separate bacterial culture (Figure 9). *P. haloplanktis* responded positively to all exudates collected from both 2 and 12 HPI in all replicate cultures (Figure 10). Responses from each biological replicate were calculated as the mean response of three technical replicates. The mean maximum $\beta(t)$ responses to exudates collected from phage-infected and uninfected cultures at 2 HPI were 0.37 (SE = 0.04) and 0.40 (SE = 0.04), respectively (Figure 10A). Mean maximum $\beta(t)$ to exudates collected from phage-infected and uninfected cultures at 12 HPI were 0.41 (SE = 0.02) and 0.26 (SE = 0.03), respectively (Figure 10B). A two-sample t-test was used to compare the maximum $\beta(t)$ responses to the exudates collected at 2 and 12 HPI as follows. Maximum $\beta(t)$ from three biological replicate chemotaxis assays were averaged to produce an overall mean response to each exudate (Figure 10C). The three overall mean responses to each exudate sample collected from phage-infected cultures were then compared against the three overall mean responses to each exudate sample collected from uninfected cultures. The maximum response to 12 HPI samples collected from phage-infected cultures was found to be statistically different than the response to samples collected from uninfected cultures at the same time point ($p = 0.0135$, $t = -4.2164$, $df = 4$, SD = 0.0420). Maximum responses between the samples collected at 2 HPI were not

statistically different (p = 0.6339, t = 0.5147, df = 4, SD = 0.0724). Comparison of maximum responses to samples from phage-infected cultures across timepoints did not show a statistical difference between 2 and 12 HPI (p = 0.4435, t = -0.8495, df = 4). Comparison of maximum responses to samples from uninfected cultures similarly did not reveal a statistically significant difference across timepoints (p = 0.05473, t = 2.6888, df = 4).

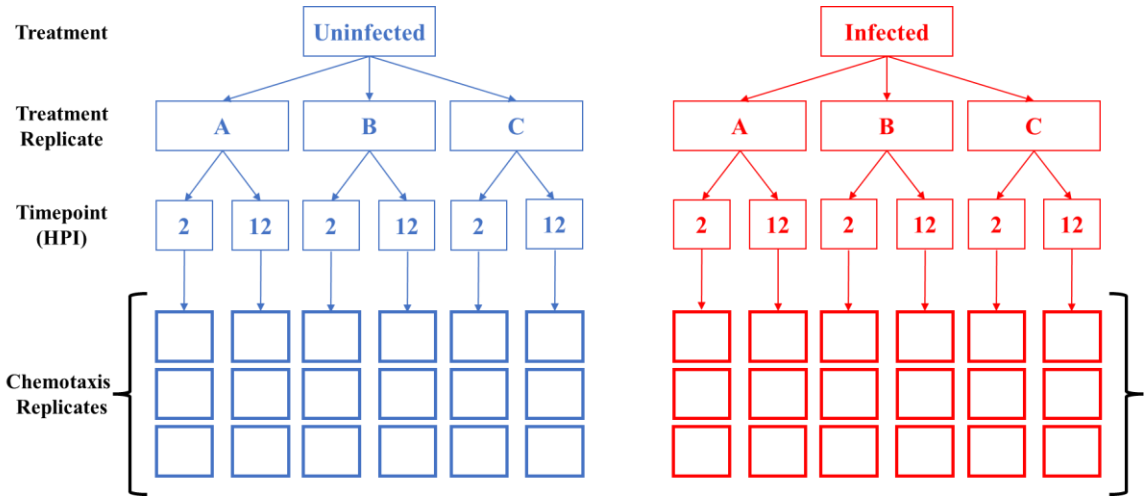

Figure 9 – Chemotaxis Experimental Outline. Diagram depicting exudate collection from uninfected and phage-infected *Synechococcus* WH8102 cultures and corresponding chemotaxis assays. Exudates were collected at two time points (2 and 12 HPI) from three replicate cultures in both treatment conditions. Three chemotaxis experiments using unique bacterial cultures were performed for each exudate sample.

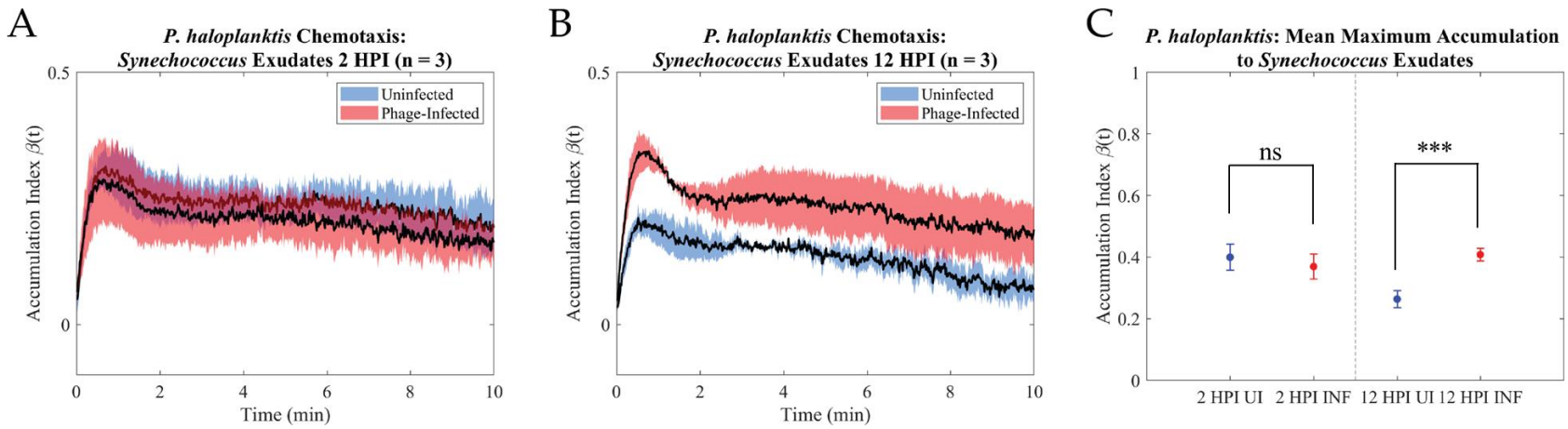

Figure 10 – *P. haloplanktis* Chemotaxis to *Synechococcus* Exudates. *P. haloplanktis* responses to exudates collected from phage-infected and uninfected cultures of *Synechococcus* WH8102 at 2 HPI (A) and 12 HPI (B). Each curve is plotted as the mean response (black lines) with the SE across biological replicates shown in the color shaded area. Three biological replicates were performed for both 2 and 12 HPI samples. Maximum accumulation responses (mean±SE) (C) to 2 HPI exudate samples from uninfected and phage-infected cultures were 0.40 ± 0.04 and 0.37 ± 0.04, respectively. Responses to 12 HPI exudate samples were recorded as 0.26 ± 0.03 and 0.41 ± 0.02 to samples collected from uninfected and phage-infected cultures, respectively (two-sample t-test *** $p \leq 0.01$).

C18 Nonpolar Metabolomics Analysis of *Synechococcus* Exudates

Analysis was performed on nonpolar compounds identified through both positive and negative electrospray ionization (ESI). ESI is a common technique utilized in MS analyses of biological samples to produce positively or negatively ionized analytes in the gas phase from liquid samples through protonation or deprotonation, respectively (76,77). Liquid samples are typically subjected to liquid chromatography prior to ESI and the data analyzed here were obtained from samples that were separated using a C18 column to extract the nonpolar fraction. The parameters used to generate the ionized analytes were previously described (46). 980 compounds were identified in total; filtering of these data as described in the methods section above yielded a list of 99 compounds. The GNPS database was then used to match this filtered list to known molecular structures. The final compound list of metabolites with known fragmentation spectra is summarized in Figure 11A as a heatmap generated in R through the ggplot2 package. 5' – Deoxyadenosine and 5' – Methylthioadenosine (MTA) were more highly abundant across all time points in the phage-infected cultures as compared to the uninfected controls. The $\log_{10}$FC of 5' – Deoxyadenosine in phage-infected exudates were 0.16, 0.17, 0.16, 0.19, 0.23, and 0.22 across 2, 4, 6, 8, 10, and 12 HPI, respectively, as compared to uninfected exudates. Thus, 5' – Deoxyadenosine was ~45 to ~70% more abundant in phage-infected exudates compared to uninfected. 5' – MTA was also detected at greater abundances across the infection (~45% to ~100% increase in phage-infected exudates over uninfected) with $\log_{10}$FC equal to 0.16, 0.22, 0.22, 0.24, 0.30, and 0.26, respectively, as compared to uninfected (Figure 11B).

A

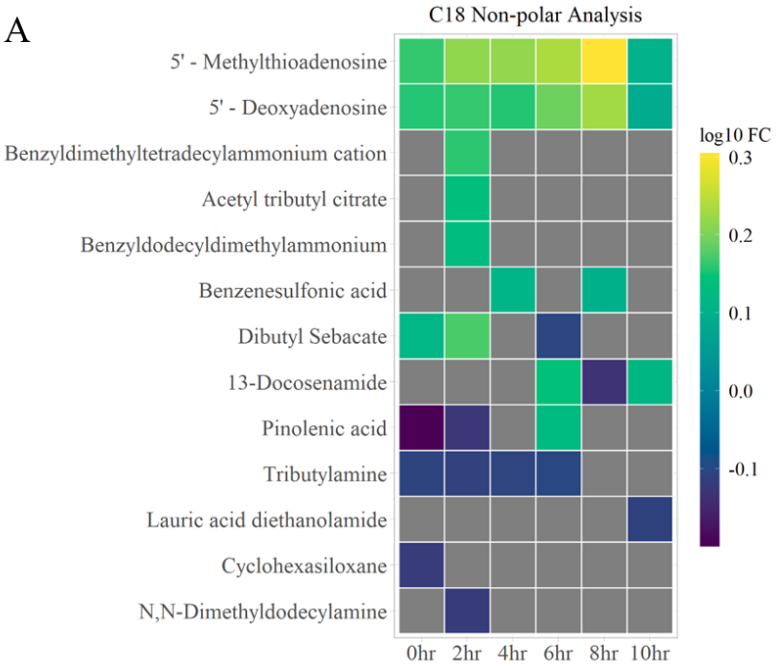

B

5' - Deoxyadenosine					
HPI	$Log_{10}FC$	*p*	BH Correction	Rank	Significant?
2	0.16	$2.0x10^{-3}$	$4.2x10^{-2}$	5	TRUE
4.4	0.17	$2.5x10^{-6}$	$8.3x10^{-3}$	1	TRUE
6	0.16	$1.2x10^{-2}$	$5.0x10^{-2}$	6	TRUE
8	0.19	$1.2x10^{-3}$	$3.3x10^{-2}$	4	TRUE
10	0.23	$1.1x10^{-4}$	$2.5x10^{-2}$	3	TRUE
12	0.22	$3.5x10^{-5}$	$1.7x10^{-2}$	2	TRUE
5' – Methylthioadenosine					
HPI	$Log_{10}FC$	*p*	BH Correction	Rank	Significant?
2	0.16	$3.1x10^{-3}$	$5.0x10^{-2}$	6	TRUE
4.4	0.22	$4.5x10^{-6}$	$2.5x10^{-2}$	3	TRUE
6	0.22	$1.2x10^{-4}$	$3.3x10^{-2}$	4	TRUE
8	0.24	$1.3x10^{-3}$	$4.2x10^{-2}$	5	TRUE
10	0.30	$7.1x10^{-8}$	$8.3x10^{-3}$	1	TRUE
12	0.26	$2.3x10^{-7}$	$1.7x10^{-2}$	2	TRUE

Figure 11 – C18 Metabolomics Analysis of *Synechococcus* Exudates. Analysis of nonpolar metabolites detected by mass spectrometry revealed differentially abundant compounds in phage-infected treatments compared to uninfected controls (A). A doubling in metabolite abundance is equivalent to log_{10} FC = 0.3. Metabolomics analysis of 5' – Deoxyadenosine and 5' – MTA (B). At all sampling time points, the log_{10}FC of both 5' – Deoxyadenosine and 5' – MTA were > 0.1 in the phage-infected treatment compared to uninfected.

DISCUSSION

Preliminary analysis of the microfluidic device and chemotaxis assay using model organisms and model chemical compounds provided control data that supported the implementation of the device and technique as tools for measuring biased motility responses in marine heterotrophic bacteria in response to various stimuli (Figure 6). These control data served to provide a measure of confidence and robustness to experimental data by providing proof of concept that these instruments could indeed be used to record and analyze cell motility patterns at the population level. Serine and phenol have been described as model chemotactic compounds for the bacterium *V. alginolyticus* (51,73,75) and serine has also been described as a chemoattractant for *P. haloplanktis* (78). However, the effect of phenol on *P. haloplanktis* has not previously been described in the literature and we did not observe a specific bias in chemotactic response to phenol at 200μM concentration.

Control experiments using *V. alginolyticus* (Figure 6A) and the model chemical attractant, serine, yielded results that were highly repeatable and representative of our expectations for data generated in these assays (51,73–75). *V. alginolyticus* responded to the serine concentration gradient within one minute in all assays. As depicted by the initial spike in β(t). This positive response continued to increase in magnitude over the course of approximately 5 minutes until plateauing before gradually returning to 0. The decline in β(t) over time was anticipated, given that diffusion is expected to disperse serine molecules across the channel as the trial progresses. The diffusion of serine across the channel due to the relaxing gradient results in *V. alginolyticus* being attracted away from the initial zone of high serine concentration. Another *Vibrio* species was shown to have rapid grow rates

(79) and suggests a potential ability of the genus to quickly take up and assimilate amino acids. Thus, it is feasible that serine concentrations become depleted due to uptake by *V. alginolyticus* as bacteria encounter the gradient. This depletion is followed by a subsequent shift in the directionality of motility as *V. alginolyticus* searches out new nutrient sources (Figure 8, Top Left Panel). The model repellant, phenol, also produced important control data to further support the veracity of the chemotactic system (Figure 8, Bottom Left Panel). A sharply repulsive effect was observed when phenol was introduced to *V. alginolyticus* as marked by a negative β(t). As the phenol gradient relaxed over time and diffused across the channel, *V. alginolyticus* were reintroduced to the negative stimulus resulting in a motility bias away from the zone of previously low phenol concentration. Finally, when *V. alginolyticus* motility was assessed in the absence of a chemical stimulus no bias in motility was observed (Figure 8, Center Left Panel) which provides strong evidence to the credibility of our assessment of chemotaxis.

P. haloplanktis consistently responded positively to serine as expected (Figure 6B) (78), however the general trend in motility responses in these assays were characteristically different than those exhibited by *V. alginolyticus*. When introduced to serine, *P. haloplanktis* responded more rapidly than *V. alginolyticus* and remained at or near peak accumulation for longer than *V. alginolyticus*. The reduction in response time may suggest greater sensitivity of *P. haloplanktis* to 200μM serine as compared to *V. alginolyticus*. *P. haloplanktis* has previously been shown to exhibit greater swimming speeds and faster response times than *V. alginolyticus* to chemical stimuli which lends support to the differences observed here (65). It is possible that although *P. haloplanktis* responds and swims faster than *V. alginolyticus* that they do not take up and deplete serine concentrations

to the same degree which could explain their prolonged accumulation state and steady reversal of motility bias throughout the time series. Somewhat surprisingly, *P. haloplanktis* were not repelled to any great degree by phenol at concentrations of 200μM. Phenols are toxic substances and are used in antimicrobials (80), however *P. haloplanktis* responses to phenol closely mirrored responses to the lack of stimulus condition, ASW.

P. haloplanktis exhibited greater chemotactic responses to *Synechococcus* exudates collected from phage-infected cultures at 12 HPI as compared to exudates collected from uninfected cultures at the same time point (Figure 10B). The observed difference in response provides novel evidence to suggest that phage-infection of *Synechococcus* has the potential to affect the chemotactic response of heterotrophic chemotactic bacteria, such as *P. haloplanktis*. These results have implications for phage influence on the transfer of nutrients throughout the marine food web. The exudate samples used in these experiments were collected from two different time points in the infection cycle and their selection was based on previous data of heightened *V. alginolyticus* responses to exudates collected from phage-infected cultures at these times (Henshaw et al., [Unpublished manuscript, in progress]). The first time point, occurred at 2 HPI at which time cell lysis had not yet begun as confirmed by flow cytometry. We did not observe a difference in the response of *P. haloplanktis* to *Synechococcus* exudates collected at this time point (Figure 10A) although two metabolites, 5' – MTA and 5' – Deoxyadenosine, were detected at statistically greater abundances in the phage-infected cultures in the nonpolar MS analysis (Figure 11). Chemotaxis experiments specifically using these two more highly abundant metabolites could reveal a chemoattractive effect on *P. haloplanktis*. Both metabolites are derivatives of the nucleoside adenosine which is a critical component of nucleic acids. 5' – MTA was

recently found to be positively associated with *Synechococcus* populations in the Atlantic (81) and preliminary experiments using *V. alginolyticus* and synthetic solutions of 5' – MTA yielded data to do indeed suggest a chemoattractive property of the metabolite (Henshaw et al., [Unpublished manuscript, in progress]). Chemotaxis is a biased random movement which is to say that the process is inherently stochastic being driven by concentration gradients. Based on the nonpolar metabolomics analysis, the $\log_{10}$FC of 5' – MTA in the phage-infected cultures compared to controls at 2 HPI was 0.17 (Figure 11B) which was the lowest detected difference across all time points and therefore may not have been present at a concentration that differentially impacted *P. haloplanktis* chemotaxis. It is also unlikely that 5' – MTA was the only stimulus, attractive or repellent, present in the exudate samples acting on *P. haloplanktis* responses. Chemotaxis is a highly dynamic process and occurs on relatively short temporal scales. Forward motility has been shown to last on the order of seconds or less in bacteria (64) and is influenced by stimulus concentrations and the duration of receptor occupancy (82–84). Phenotypic diversity across individuals within a bacterial population also contributes to cell-to-cell variability in response. The accumulation parameter, $\beta(t)$, defines chemotactic responses at the population level and therefore does not describe the potential variation in responses at the single cell level. Along with intrapopulation variation it follows that chemosensitivity can vary in a concentration dependent and interspecies manner (85). Indeed, this was observed in our initial control experiments where 200μM phenol was highly repellent to *V. alginolyticus*, but not to *P. haloplanktis* (Figure 6). Thus, it is not necessarily surprising that we did not observe identical chemotactic responses of these two bacterial species to the same *Synechococcus* exudates. *V. alginolyticus* responded more strongly to

Synechococcus exudates from both phage-infected and uninfected cultures (Henshaw et al., [Unpublished manuscript, in progress) as compared to *P. haloplanktis,* however populations of both bacterial species were attracted to these samples. Differences in chemotactic response to a substrate is not unprecedented and has previously been shown in *V. alginolyticus* and *P. haloplanktis* (65,86). Indeed, a stimulus may serve as an attractant to an organism while being inert or having a dichotomous effect on various other organisms (85). The complexity with which these interactions can occur has ecological implications in the context of microbial population dynamics and the relative success of one species over another (66,87,88). If a particular heterotrophic organism is more adept at navigating to metabolites that are manipulated during phage-infection, then perhaps it is more likely for these species to outcompete others during infection conditions.

At 12 HPI, cells have begun lysing and releasing intracellular components into the media. The assumption then, is that concentrations of bioavailable labile molecules are increased at this time point compared to at 2 HPI and whole exudate samples are therefore likely to contain increased metabolite concentrations. *P. haloplanktis* were observed to be significantly more attracted to exudate samples collected from phage-infected cultures compared to uninfected cultures at this later time point. Maximum responses to 12 HPI exudate samples from phage-infected cultures were on average 1.5x greater than the maximum responses to samples collected from uninfected cultures (Figure 10C). Additionally, *P. haloplanktis* displayed greater sustained accumulation on the left side of the microfluidic channel, where exudates were initially injected, in response to the samples collected from phage-infected cultures compared to samples from uninfected cultures. One potential rationale for the sustained accumulation observed in response to samples from

both timepoints is that the attractive stimuli is not depleted, or potentially even metabolized, by *P. haloplanktis* (89). If the attractant compound(s) in the exudate are not taken up, it is conceivable that *P. haloplanktis* remains localized in the area of the attractant due to increased run-reversals in response to higher attractant concentration. Alternatively, as rates of molecular diffusion are dependent on mass, it is possible that the metabolite(s) attracting *P. haloplanktis* have a lower diffusion coefficient and therefore diffuse more slowly across the channel. Also of note, the maximum mean response of *P. haloplanktis* to exudates collected from uninfected cultures at 12 HPI was lower than responses to exudates collected from the same treatment at 2 HPI. Although this difference was not statistically different ($p = 0.06$), a reduction in maximum accumulation could result due to shifts in metabolite abundances of key chemostimuli across timepoints. Direct comparisons in the chemotactic response of *P. haloplanktis* to exudates collected from phage-infected and uninfected cultures were attempted by means of competition style experiments where via introduction to both exudate types simultaneously. However, results obtained from those experiments were highly variable resulting in a lack of statistically significant differences between bacterial responses to the different treatments.

The results of these experiments suggest that cyanophages can indirectly influence chemotactic responses of the marine heterotrophic bacterium *P. haloplanktis* through alterations in metabolites released from phage-infected *Synechococcus* host cells during cell lysis. This lends support to a concomitant role of cyanophage infection on microbial interactions and nutrient flux. Bacterial chemotaxis to algal exudates and lysis products has previously been shown (62,64,65,90), but as of this work the effect of viruses on this interaction has not been investigated. Culture exudates of *Synechococcus* WH8102

infected with the cyanophage S-SSM5 collected at 12 HPI were found to elicit stronger chemotactic responses as compared to exudates collected from uninfected cultures collected at the same time point. Although we did not detect chemotactic variation to the exudate samples collected at 2 HPI, the experimental and analytical parameters used here are designed to measure population responses and cannot account for heterogeneity within the population at the individual cell level (91). Modeling of data such as frequency of reversals, cell velocity, and response time may yield more information regarding variability in chemotactic responses at the individual cell level (66,82,84,92), but accurate collection and interpretation of these measurements requires greater temporal resolution beyond the scope of these experiments. Further investigation of bacterial responses to the compounds identified through the MS analysis could also help to elucidate potential drivers of chemotaxis and may reveal in more detail specific phage manipulations of the host that induce observed responses.

CH II: BACTERIAL CHEMOTAXIS TO PHAGE-INFECTED *SYNECHOCOCCUS*

INTRODUCTION

Viral abundance in the oceans has been reported to reach concentrations ranging from ~10^6 to 10^8 viruses mL^{-1} making them the most abundant biological entities in the marine ecosystem (10,93,94). It is estimated that viruses lyse ~20% of marine bacterial populations per day (95) making them influential ecosystem components. The viral shunt and viral shuttle hypotheses (13,96) suggest a critical role of marine viruses in nutrient flux and carbon sequestration. Viral lysis of infected cells releases both dissolved organic matter (DOM) and particulate organic matter (POM), the difference between which is operational with the two generally being distinguished by a size threshold of 0.2μm (POM > 0.2μm) (14). Cell bodies and fragments in addition to fecal pellets are examples of POM (97). A proportion of DOM released due to viral lysis is labile (31,98–100) and heterotrophic microbes are able to rapidly acquire and assimilate these usable nutrients which stimulates their growth and shunts these compounds away from higher trophic levels (13,30,96,101). Labile DOM can also be released from POM and can be an important nutrient source for heterotrophic bacteria (63,102,103). Conversely, some types of POM released upon lysis may be recalcitrant, persisting longer in the water column, and these carbon-rich compounds are more likely to sink and be sequestered in the ocean interior due to their greater size, density, and resistance to degradation (30,104). Some types of DOM may also be recalcitrant (30). Viruses therefore likely contribute to the biological carbon pump, as described in Chapter I, by facilitating the generation of sinking particles thereby enhancing carbon sequestration (13,96). Marine viruses may also influence upward trophic transfer

of nutrients by influencing predator grazing rates on virally-infected phytoplankton (27,28).

Marine phytoplankton constitutively exude metabolites that form nutrient rich microzones (also called the "phycosphere") surrounding the cell (11,106–108) which can facilitate bacterial growth and influence microbial community composition (16,109). Heterotrophic bacteria are able to detect these nutrients through membrane bound receptors that initiate chemotactic responses (described in Chapter I: Introduction, p.6-8). Modeling has provided insight into theoretical phycosphere size ranges, nutrient concentrations, and molecular diffusivity of dissolved compounds that may be found in the phycosphere (107,110,111). It has generally been thought that phytoplankton with a cell diameter ≤ ~1μm (such as *Synechococcus*) produce phycospheres of negligible size (87,107). However, positive marine bacterial chemotaxis has been reported in response to exudates collected from uninfected phytoplankton cultures including *Synechococcus* and *Prochlorococcus*, another ecologically important cyanobacteria of cell diameter ~1μm, (63–65,86,90,112) and other live uninfected phytoplankton (53,62). Recently, quantification of direct nutrient exchange between *Synechococcus* and a chemotactic bacterium was reported (66) and presents a paradigm shift in our understanding of nutrient exchange possibilities. The ability of bacteria to chemotactically interact with and respond to *Synechococcus* and their exudates suggests a potential for differential responses under phage-infection conditions. As of this writing, however, no published data exist quantifying chemotactic responses to virally-infected phytoplankton or their exudates. The data presented in Chapter I: Results provide new evidence that bacteria display enhanced

chemotaxis in the presence of exudates collected from phage-infected cultures as compared to exudates collected from uninfected cultures.

In the following experiments, cultures of *Synechococcus* sp. WH8102 were infected with the cyanophage S-SSM5 and the responses of the model chemotactic marine bacterium *V. alginolyticus* were quantified in response to both phage-infected and uninfected *Synechococcus* cells at environmentally relevant concentrations. *V. alginolyticus* were found to chemotax more strongly to intact phage-infected *Synechococcus* cells as compared to uninfected cells providing novel experimental evidence of viral influence on microbial interactions. These results suggest that the cyanophage S-SSM5 alters *Synechococcus* host metabolic exudates to a degree that is detectable by *V. alginolyticus* prior to viral-induced lysis which has the potential to alter our understanding of viral controls on microbial interactions and nutrient flux.

MATERIALS AND METHODS

Bacterial Growth Conditions and Media

V. alginolyticus cultures were grown and suspensions prepared as previously described in Chapter I: Materials and Methods.

Synechococcus WH8102 Growth Conditions and Media

Synechococcus WH8102 (CCMP2370, NCMA Bigelow) were grown in SN media prepared in artificial seawater (ASW) (Table I) (67,68). Batch salt solutions were prepared in 20L carboys. 500mL of anhydrous salt solution and 250mL of hydrous salt solution were combined and pH adjusted as needed to ~8.2. Solutions were autoclaved and nutrients added to create SN media. Milli-Q water was then added to a final volume of 1L. SN nutrient component stocks were stored at 4°C in the dark and were syringe filtered (0.2μm) prior to their addition to ASW to make the final SN media. Media pH was confirmed following addition of all nutrients. Cultures were grown in sterile 40mL ($25cm^2$) polystyrene cell culture flasks (Greiner Bio-One, Frickenhausen, Germany #690160) at 22°C on a 14/10 light/dark cycle at 50μmol m^{-2} s^{-1}. Culture growth and concentration was tracked using a SpectraMax ID3 plate reader to measure culture absorbance (440nm) and fluorescence (440/680nm & 537/577nm) in conjunction with cell counts determined by flow cytometry as described below.

Artificial Seawater (ASW)			
Anhydrous Salts (20L)			
Salt	**Mass (g)**		
NaCl	706.5		
Na2SO4	118.3		
KCl	19.97		
Na2CO3	5.8		
KBr	2.87		
H3BO3	0.77		
NaF	0.1		
Hydrous Salts (10L)			
MgCl2 ● 6H20	319.733		
CaCl2 ● 2H20	44.8		
SrCl2 ● 6H20	0.727		
SN Media Nutrients			
Component	**Stock Concentration (g L-1)**	**Volume (mL)**	**Final Concentration (M)**
NaNO3	76.5	10	9.0x10-3
K2HPO4	15.68	1	9.9x10-5
Na2EDTA ● 2H2O	5.58	1	1.5x10-5
Na2CO3	10.7	1	1.0x10-4
B12	0.01	1	7.38x10-10
Trace Metal Soln.		1	--
Trace Metal Solution			
Component	**Mass (g)**	**Final Concentration (M)**	
Citric acid ● H2O	6.25	3.25x10-5	
Ferric ammonium citrate	6	--	
MnCl2 ● 4H2O	1.4	7.08x10-6	
Na2MoO4 ● 2H2O	0.39	1.61x10-6	
ZnSO4 ● 7H2O	0.222	7.72x10-7	
Co(NO3)2 ● 6H2O	0.025	8.59x10-8	

Table I – Artificial Seawater and SN Media Recipe.

Flow Cytometry

Autofluorescent *Synechococcus* were counted using a Beckman Coulter CytoFLEX flow cytometer (Figure 12A). Calibration with CytoFLEX Daily QC Fluorospheres with the appropriate detector configuration (described below) was performed prior to each use. For *Synechococcus* samples, three replicate blanks were performed using both 0.2µm filtered natural seawater and 0.2µm filtered SN media (Figure 12B). Detections within gated populations were averaged for each blank type and then summed together before

subtracting from gated cell counts to correct for background signal. All samples were run at a flow rate of 10μL min^{-1} for 10 minutes or until ≥ 10,000 gated events were recorded. Chlorophyll-a pigments were excited via blue laser (488nm) and emission was detected using a 690/50nm filter (Blue690) with a gain setting of 250. Cell size was determined via violet laser (405nm) and detected by a 405/10nm filter (Violet SSC) with gain set to 100. Threshold for counts was manually set to a minimum of 1,000 triggered on Blue690 with width set to Violet SSC.

Phage particles were quantified (Figure 12C) in samples stained with SYBR Green I (Invitrogen, Eugene, OR, #S7563) (113,114). The stock solution (10,000x in DMSO) was diluted 1:200 in Milli-Q water to make the working solution. Autoclaved TE buffer (pH 8.0, 10mM Tris, 1mM EDTA) (VWR, Radnor, PA #E112) was 0.2μm filtered prior to use for background signal correction and diluting stained samples (Figure 12D). 5μL of the SYBR Green I working stock were added to three individual 500μL TE blank samples. Blanks were incubated at 80°C in the dark for 10 minutes, then allowed to cool on the bench for 5 minutes prior to acquisition. Both Milli-Q water samples and stained TE blank samples were confirmed to have < 50 events per second prior to running any experimental samples. Experimental samples were fixed in a final concentration of 0.5% glutaraldehyde and flash frozen in liquid nitrogen upon collection before being stored at -80°C. Samples were thawed on ice after confirming cleanliness of the flow cytometer and acquiring blank data. Samples were diluted in 0.2μm filtered TE buffer to a final volume of 500μL and were stained with 5μL of the SYBR Green I working stock. Stained samples underwent the same incubation procedure as the TE buffer blanks. A 488nm laser was used in conjunction with a 525/40nm emission filter to capture fluorescent signal. Phage data were recorded

using Blue525 and Violet SSC gain settings of 50 and 100, respectively. The primary threshold channel was set for Blue525 with a manual threshold of $1x10^3$ and width set to Violet SSC. Count data were subsequently analyzed in FlowJo.

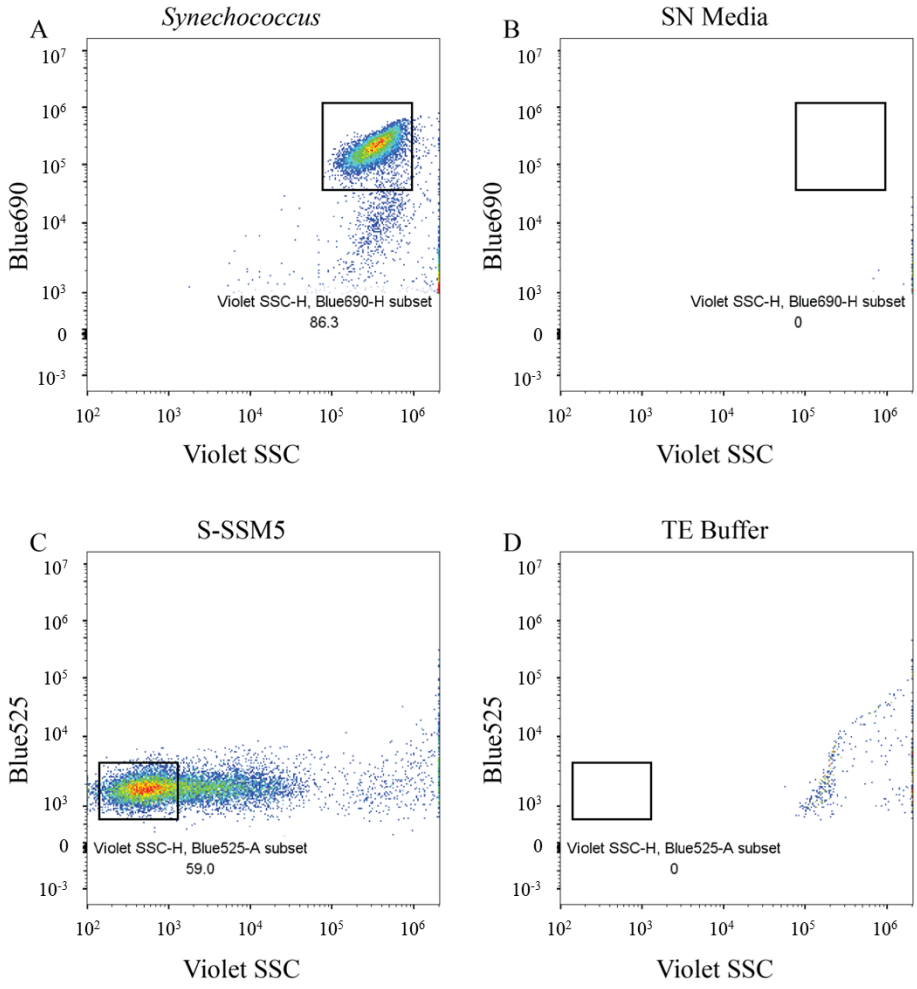

Figure 12 – Cell, Phage, and Negative Controls for Flow Cytometry. Representative FCM plots with gates used to quantify cell and phage concentrations: *Synechococcus* cell population (A), SN media negative control (B), cyanophage S-SSM5 positive control (C), and TE Buffer negative control (D).

Generation of Phage Stock

Synechococcus WH8102 cultures were infected in triplicate at a concentration of $4.3x10^7$ cells mL^{-1} in 40mL of SN media with 4mL of a pre-existing S-SSM5 phage stock at a concentration of $1.45x10^8$ PFU mL^{-1} (MOI ~0.3:1). Cell and phage concentrations were quantified by flow cytometry (data not shown) to track infection dynamics throughout the time course. Progeny phage were isolated from infected cultures at 36 HPI by filtration using 0.2μm PES filters. The newly generated phage stock was then concentrated using Amicon Ultra – 15 centrifugal filters with a 50kDa molecular weight cutoff (Millipore, Tullagreen, Carrigtwohill, Co Cork IRL, #UFC905024). Amicon filters were precoated with 1% BSA in PBS for 5 – 10 minutes prior to phage stock concentration. The concentrated stock titer was determined by plaque assay as described below.

Plaque Assay

Infectious phage titer was determined by plaque assay method. Triplicate samples of S-SSM5 phage stock were 10-fold serially diluted in a final volume of 1mL SN media to a final dilution of 10^{-9}. *Synechococcus* WH8102 cells were homogenized with diluted phage samples to a final concentration of ~$5x10^7$ cells mL^{-1} in 20mL 0.8% LMP agarose (Invitrogen, Eugene, OR, #16520) dissolved in SN media. Prior to solidification of the agarose mixture, solutions were poured onto 20mL 0.8% base layer LMP agarose plates in 100x15mm petri dishes (VWR, Radnor, PA, #25384-342). Phage dilutions were plated with cells in triplicate. Plates were incubated at 22°C on a 14/10 light/dark cycle at 50μmol m^{-2} s^{-1} and were monitored daily for plaque formation. Plaques were counted additively as they appeared. Plates from a single phage dilution that had between 50-100 plaques were used to calculate the infectious phage titer of the original stock by first averaging the total

plaque count across triplicate plates. The average was then divided by the volume of phage plated to yield the number of plaque forming units (PFU) per volume. The resulting PFU mL^{-1} were multiplied by the dilution factor to give the infectious titer in the original undiluted stock.

Infection Assays and Sampling

Both control uninfected and phage-infected experiments were performed identically with the exception that in uninfected replicates phage addition was substituted with an equivalent volume of SN media. All infection experiments were performed within a week using the same phage stock. The infectious phage titer of the stock was calculated to be $1.4x10^8$ PFU mL^{-1} by plaque assay method (described above) with *Synechococcus* WH8102 as the host (Figure 13). Cell cultures were diluted with fresh SN media to a cell concentration of $7\text{-}9x10^5$ cells mL^{-1} the day prior to the experiment from cultures growing in exponential phase. Prior to the beginning of the light cycle, *Synechococcus* culture concentrations were confirmed via flow cytometry and adjusted to $\sim1x10^6$ cells mL^{-1} as necessary with fresh SN media. At the beginning of the light cycle, a calculated volume of phage stock, or media for uninfected controls, was added to achieve a target multiplicity of infection (MOI) of 3:1. For the first 45 minutes immediately following phage or media addition, cultures were mixed for 1 minute at 5-minute intervals in 50mL conical tubes (VWR, Radnor, PA, #89039-658) to promote phage adsorption to cells. After 45 minutes, *Synechococcus* cultures were centrifuged at 2,000xg for 15 minutes at 20°C. Supernatants were decanted and cells were resuspended in a volume of fresh media equal to the starting culture volume and transferred to sterile, pre-autoclaved 50mL glass flasks. At 3- and 7-hours post-infection (HPI), live cell concentration was assessed by flow cytometry and

10mL of *Synechococcus* cells were collected from cultures for chemotaxis assays. 100µL samples were also taken and fixed in 0.5% glutaraldehyde for later cell and phage quantification. Cells collected for chemotaxis assays were centrifuged at 2,000xg for 15 minutes at 20°C in 15mL conical tubes (VWR, Radnor, PA, #89039-666). The cell pellet was then washed in 10mL of ASW and centrifuged again. The final cell pellet was resuspended in 1mL of ASW, cell concentration quantified by flow cytometry, and the suspension volume was adjusted as necessary to a final concentration of ~3-4x10^5 cells mL^{-1}. Following cell suspension preparations, chemotaxis assays were run at 4 and 8 HPI (Figure 14). Additional samples were collected and fixed in 0.5% glutaraldehyde at 1, 3, 5, 7, 8, 9, 10, 11 and 25 HPI for quantification of cell and phage concentrations. Fixed samples were flash frozen in LN2 in 2mL cryovials (Corning, Sunnyvale, CA, #430488).

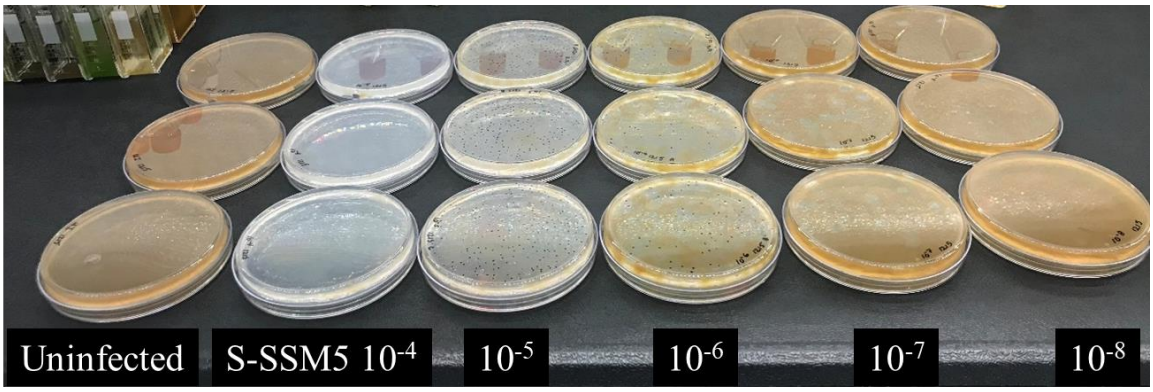

Figure 13 - Plaque Assay to Determine Infectious Titer of S-SSM5 Phage Stock. Lower phage dilutions result in greater cell lysis evidenced by increased clearance of the bacterial lawn. The number of infectious phage particles were enumerated by counting distinguishable plaques at higher phage dilutions.

Chemotaxis Assay

Hamilton gas tight syringes and the microfluidic channel were prepared as previously described in Chapter I: Materials and Methods. Syringe pump settings were also held constant from section I methods (flow rate of 25μL min^{-1} run for 5 minutes to establish gradient before stopping flow for data collection). *Synechococcus* cells were injected into the left side of the channel at a concentration of ~10^5 cells mL^{-1}, *V. alginolyticus* into the center inlet at concentrations of ~10^9 cells mL^{-1}, and ASW into the right. Images were collected over a 60-minute time period at 1FPS using the FLIR Grasshopper 3 monochrome camera (Teledyne FLIR, Wilsonville, OR #GS3-U3-51S5M-C). To verify *Synechococcus* cell positions in the device, fluorescence images were captured immediately prior to and following the 60-minute time series (Figure 15). A 488nm laser was used to excite the autofluorescent *Synechococcus* cells and a custom filter cube incorporating a 447/60nm excitation and 520nm longpass emission filter was built to facilitate visualization of *Synechococcus* positions. Image analysis in MATLAB was performed as previously described in Chapter I: Materials and Methods.

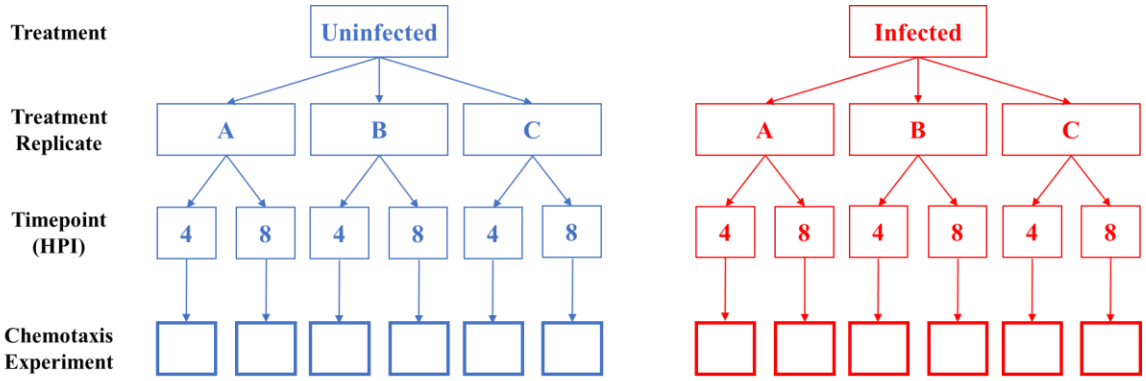

Figure 14 – Experimental Outline: Chemotaxis to Intact *Synechococcus*. Three independent replicate experiments were performed for both uninfected and phage-infected *Synechococcus* for a total of six experiments. For each replicate experiment, *Synechococcus* cells were collected at two time points, 3 and 7 HPI, for analysis of *V. alginolyticus* chemotaxis responses. In each chemotaxis experiment, images were collected for 60 minutes at a frame rate of 1FPS.

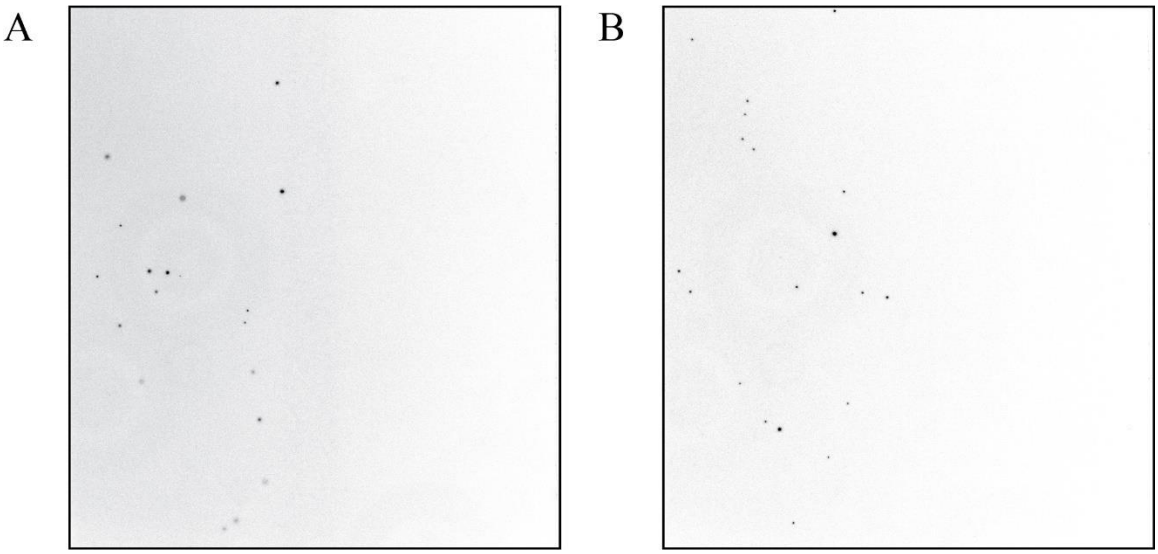

Figure 15 – Fluorescence Imaging in the Microfluidic Device. Representative fluorescence images of *Synechococcus* cells within the microfluidic device prior to (A) and following (B) each chemotaxis experiment. Images were inverted, then enhanced for brightness and contrast in ImageJ for presentation purposes. Black spots in each image are *Synechococcus* cells. Pairwise t-tests performed on *Synechococcus* cell counts for both uninfected and phage-infected treatments showed no statistical difference between the number of cells at the beginning and end of each 60-minute period at both 3 and 7 HPI ($p \geq 0.70$).

RESULTS

Tracking of *Synechococcus* Culture Concentration by Flow Cytometry

Concentrations of *Synechococcus* WH8102 were determined by flow cytometry throughout each experiment (Figure 16). Seed culture concentrations were similar across all experiments (mean = $7.83 \times 10^7 \pm$ SE = 3.59×10^6 cells mL^{-1}). The mean concentration of diluted seed cultures was $8.59 \times 10^5 \pm$ SE = 3.34×10^4 cells mL^{-1}. The mean initial cell concentration prior to the start of each experiment was $1.08 \times 10^6 \pm$ SE = 1.26×10^5 cells mL^{-1} in uninfected experiments and $1.05 \times 10^6 \pm$ SE = 1.20×10^4 cells mL^{-1} in phage-infected experiments. Following phage adsorption, cells were centrifuged and resuspended in fresh SN media to $4.1 \times 10^5 \pm$ SE = 4.71×10^4 cells mL^{-1} and $6.35 \times 10^5 \pm$ SE = 1.50×10^5 cells mL^{-1} in uninfected and phage-infected experiments, respectively. A two-sample t-test showed no significant difference in cell concentrations across treatments following resuspension (t = -1.4356, df = 2.3924, p = 0.268).

3 and 7 HPI were selected for chemotaxis experiments as previous data suggested that these represented early-middle and late stages of the latent period of infection prior to cell lysis. *Synechococcus* suspension concentrations for both chemotaxis timepoints were quantified by flow cytometry. Mean cell concentrations of uninfected suspensions used in chemotaxis assays at 3 and 7 HPI were $3.37 \times 10^5 \pm$ SE = 6.74×10^4 cells mL^{-1} and $2.91 \times 10^5 \pm$ SE = 8.50×10^4 cells mL^{-1}, respectively. For phage-infected cells, means of suspensions used for chemotaxis at 3 and 7 HPI were $2.79 \times 10^5 \pm$ SE = 8.35×10^3 cells mL^{-1} and $3.05 \times 10^5 \pm$ SE = 7.74×10^4 cells mL^{-1}, respectively. A pairwise t-test with Benjamini – Hochberg correction applied showed no significant difference in cell concentrations of *Synechococcus* suspensions between treatments or time points (p = 0.91).

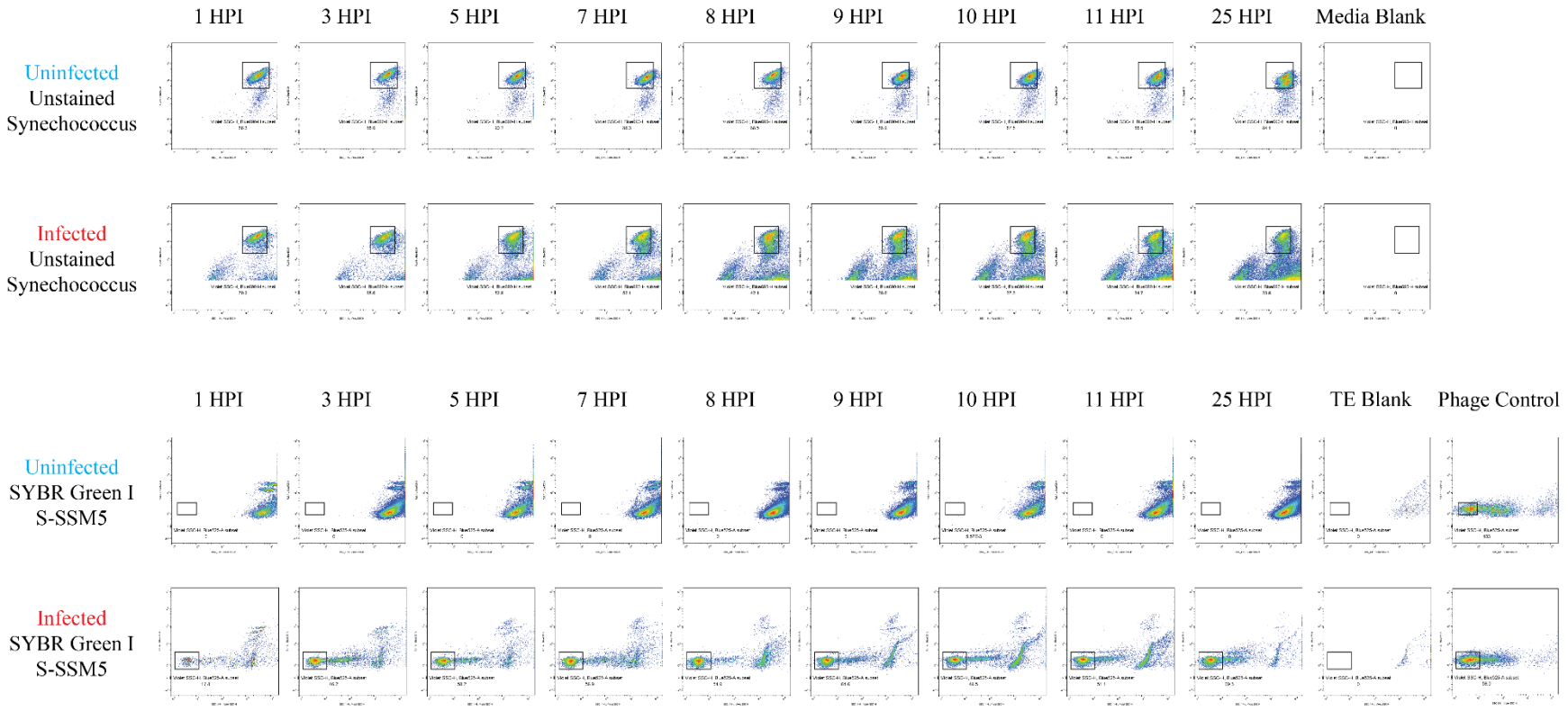

Figure 16 –Monitoring of Infection Dynamics in *Synechococcus* Cultures by Flow Cytometry. Flow cytometry data from one representative replicate of uninfected and phage-infected cultures. Autofluorescent *Synechococcus* cells were quantified in unstained samples. Phage samples were quantified from samples stained with SYBR Green I.

Infection Dynamics of S-SSM5 in *Synechococcus* WH8102

Samples were collected, fixed in 0.5% glutaraldehyde, and flash frozen in LN2 to track the infection by flow cytometry over the course of each experiment (Figure 17). Uninfected culture concentrations did not change significantly over 25 hours (t = -0.35526, df = 3.8028, p = 0.7412) (Figure 17A). Phage-infected cultures declined in concentration over the same time period (Figure 17B). Individual percent changes in cell concentration over time for each experiment are summarized in Table II. Phage-infected cell culture concentrations declined an average of 6% between 1 HPI (initial concentration following resuspension in fresh media) and 3 HPI though this difference was found to not be significant when comparing across time points using a pairwise t-test with Benjamini – Hochberg correction (p = 0.58). At 7 HPI, an average decline of 40% compared to 1 HPI was observed in cell cultures infected with S-SSM5. At 7 HPI, the percent of cells remaining in phage-infected cultures was found to be significantly different from both the 1 and 3 HPI samples (p = $3.7x10^{-3}$ and $1.1x10^{-2}$, respectively). By 25 HPI, an average decrease of 76% was recorded for phage-infected cultures.

Phage particles were not detected in uninfected cultures above negligible quantities likely due to background signal slightly above TE blanks (Figure 17C). At 1 HPI, the mean phage concentration was $3.82x10^{6} \pm SE = 1.47x10^{6}$ phage mL^{-1}. At 3 HPI, the mean phage concentration was $4.57x10^{6} \pm SE = 2.52x10^{6}$ phage mL^{-1} and was not significantly different from 1 HPI by two-sample t-test (t = -0.25504, df = 3.2231, p = 0.8141). Mean phage concentration at 7 HPI was $6.17x10^{6} \pm SE = 2.22x10^{6}$ phage mL^{-1} which was also not significantly different from 1 HPI (t = -0.8805, df = 3.4743, p = 0.4353). At 25 HPI, the mean phage concentration was $1.59x10^{7} \pm 5.5x10^{6}$ phage mL^{-1} (Figure 17D).

Relative Percent Cell Concentration

Time (Hours)	0	2	4	6	7	8	9	10	24
UI Exp01	100%	126%	116%	110%	112%	109%	119%	116%	121%
UI Exp02	100%	123%	95%	107%	104%	100%	87%	100%	101%
UI Exp03	100%	92%	ND	95%	ND	ND	ND	ND	91%
INF Exp01	100%	92%	76%	43%	40%	28%	27%	26%	18%
INF Exp02	100%	96%	87%	77%	73%	65%	63%	55%	29%
INF Exp03	100%	91%	76%	57%	58%	46%	43%	39%	25%

Table II – *Synechococcus* Relative Cell Concentrations. *Synechococcus* cell concentrations in uninfected (UI) and phage-infected (INF) treatments were determined by flow cytometry from samples fixed in 0.5% glutaraldehyde. Each row shows the normalized cell concentrations in each experiment over time expressed as a percent of cells relative to time = 0 hours. Percent values were calculated by dividing the cell concentration at each sampling time by the starting concentration in each experiment at 0 hours. ND = no data.

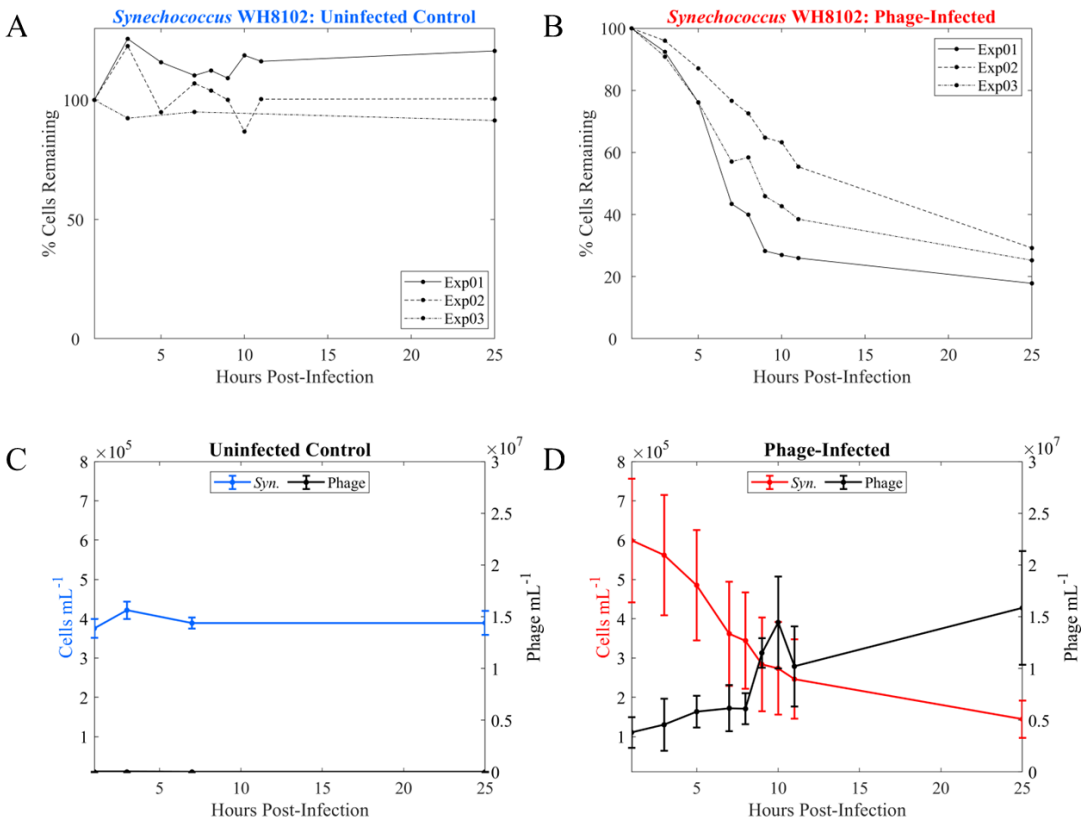

Figure 17 – *Synechococcus* WH8102 and S-SSM5 Infection Dynamics. Percent cell concentrations were computed relative to the initial concentration for uninfected (A) and phage-infected (B) treatments by dividing cell concentrations at each time point by the initial concentration at 0 hours. The mean ± SE cell and phage concentrations of triplicate experiments were calculated for uninfected (C) and phage-infected (D) treatments. Relative cell concentrations at 3 HPI were not significantly different from starting concentrations in phage-infected cultures (p = 0.58), but were significantly different at 7 HPI (p = 3.7x10^{-3}) as determined by pairwise t-test with Benjamini – Hochberg correction. Phage concentrations at 3 and 7 HPI were not significantly different from starting concentrations (p = 0.81 and 0.44, respectively).

V. alginolyticus Chemotactic Responses to Intact *Synechococcus* WH8102

Chemotaxis experiments were run at 4 and 8 HPI following preparation of *Synechococcus* suspensions of cells collected at 3 and 7 HPI. Mean accumulation responses and SE of *V. alginolyticus* to uninfected and phage-infected cells at each time point were calculated and plotted (Figure 18A&B). As in section I, accumulation of cells is represented by the variable β(t) and is calculated in the same way as described in section I methods. Overall maximum responses (Figure 18C) of *V. alginolyticus* to uninfected and phage-infected cells at 4 HPI were 0.09 ± SE = 0.00 and 0.49 ± SE = 0.22. A two-sample t-test between responses at 4 HPI indicated no significant difference based on α = 0.05 (p = 0.0868, t = -2.2588, df = 4). Maximum responses of *V. alginolyticus* at 8 HPI were 0.23 ± SE = 0.12 and 0.67 ± SE = 0.06 to uninfected and phage-infected *Synechococcus* cells, respectively, and were found to be statistically different (p = 0.02735, t = -3.397, df = 4).

Analysis of mean β(t) values in each treatment with respect to time showed that at 4 HPI, *V. alginolyticus* mean accumulation to phage-infected *Synechococcus* peaked at t = 397s (β(t) = 0.42). At the same time, the maximum mean accumulation to uninfected cells was 8.4x lower with β(t) = 0.05 (Figure 18A). At 8 HPI, the maximum mean accumulation with respect to time in response to phage-infected cells occurred at t = 451s (β(t) = 0.64) while only measuring 0.08 in response to uninfected cells marking an 8x greater maximal response to phage-infected cells at 8 HPI (Figure 18B).

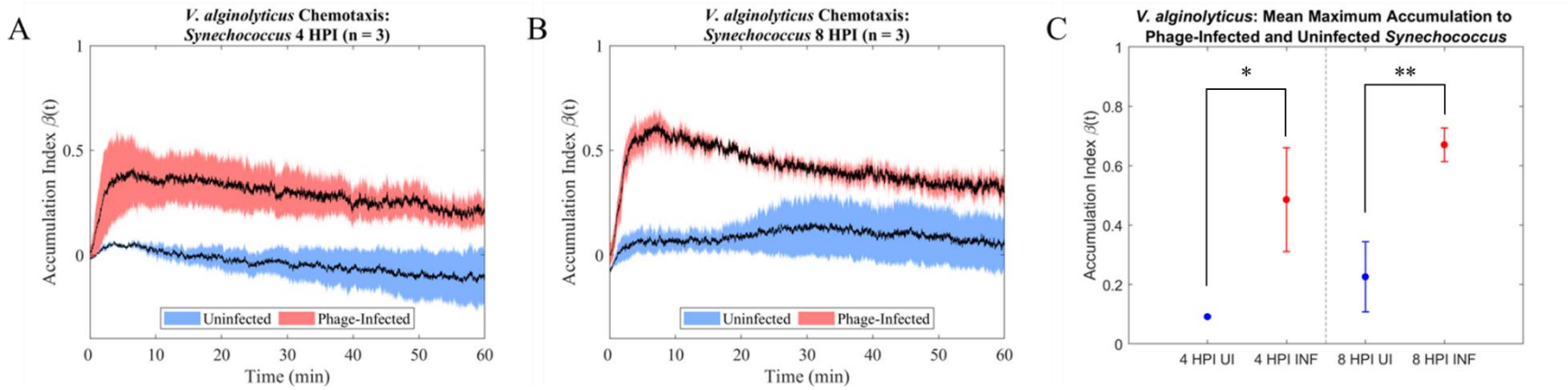

Figure 18 – *V. alginolyticus* Chemotaxis to Intact-Phage-Infected *Synechococcus*. Chemotactic responses of *V. alginolyticus* at 4 HPI (A) and 8 HPI (B). Mean responses (black lines) and SE (shaded area) to uninfected (blue) and phage-infected (red) *Synechococcus* cultures were calculated from three independent experiments using unique bacterial cultures. Maximum β(t) for each experimental treatment and timepoint were calculated as a mean of three independent replicates (C). The error bars represent SE in each group. A two-sample t-test comparing responses to uninfected and phage-infected cells at each time point revealed no statistical difference at 4 HPI (* $p \leq 0.1$), but a significant difference in chemotactic response was found at 8 HPI (** $p \leq 0.05$). Comparison of maximum responses within treatments, across timepoints, showed no statistical difference in responses to uninfected cells ($p = 0.3$) or phage-infected cells ($p = 0.4$) at 4 and 8 HPI.

DISCUSSION

V. alginolyticus responded positively to phage-infected *Synechococcus* at environmentally relevant concentrations (~10^5 cells mL^{-1}) and exhibited prolonged accumulation through 60 minutes in all experimental replicates at both time points (Figure 18). Increased and prolonged bacterial accumulation may indicate that phage-infected *Synechococcus* are releasing attractive chemical stimuli at greater concentrations or higher rates than uninfected cells which can influence *V. alginolyticus* localization. *Synechococcus* cells were washed in ASW prior to chemotaxis assays. Thus, the observed attraction and accumulation of *V. alginolyticus* in response to *Synechococcus* cells occurred in response to metabolites actively exuded from *Synechococcus* cells. Previous studies have reported prolonged bacterial accumulation in response to uninfected phytoplankton (52) and synthetic nutrient sources up to hundreds of seconds (78). Modeling and simulations of bacterial chemotaxis in response to phytoplankton cells have characterized the potential of phytoplankton exudates to initiate bacterial clustering around nutrient sources (106,115). The mean peak chemotactic responses observed here occurred relatively early in each time series at t = 397s and 451s, out of a total duration of 3,600s (60 minutes), for *Synechococcus* cells collected at 3 HPI and 7 HPI, respectively. The elapsed time to reach maximum accumulation to *Synechococcus* cells collected at 3 HPI (mean = 506s $\pm$ SE = 155s) and 7 HPI (mean = 463s $\pm$ SE = 68s) was not significantly different (p = 0.82). Additionally, fluorescence images taken prior to and following each 60-minute chemotaxis experiment showed that the total number of *Synechococcus* cells within the field of view did not significantly decrease during the course of each experiment ($p \geq 0.70$ for all comparisons). These results provide evidence that intact phage-infected *Synechococcus*

released exudates that attracted *V. alginolyticus* to a greater degree than intact uninfected *Synechococcus*.

Phytoplankton exudates can contain various compounds (11,116–118) which may differentially affect bacterial chemotaxis (65,78,85). Whether the observed difference in chemotaxis to phage-infected and uninfected *Synechococcus* was due to increased rates of exudation or increased concentrations of attractive exudates being released is unclear. The nonpolar MS analysis conducted in section I of this thesis identified two compounds, 5' – MTA and 5' – Deoxyadenosine, that were more highly abundant across all sampling time points in phage-infected cultures of *Synechococcus* WH8102 compared to uninfected *Synechococcus* cultures (Figure 13). 13 metabolites were identified in the nonpolar analysis as differentially abundant between the two treatments. 29 known metabolites were differentially abundant in the polar analysis between treatments (46). The heterogeneity of detected metabolites in *Synechococcus* exudates evidences the potential for variability in chemotactic responses. Though metabolites were not directly quantified here, a series of chemotaxis experiments could be performed using synthetic versions of the previously identified compounds at varying dilutions to determine their attractiveness and limits of detection to *V. alginolyticus*. Additional nucleotides, amino acids, and their derivatives were identified in the polar MS analysis conducted on the same experimental cultures (46) and could also be investigated for chemoattractive properties. A microfluidic device that is capable of performing automatic and intrinsic serial dilutions could greatly increase throughput of such experiments (74). Indeed, *V. alginolyticus* were found to respond in a concentration dependent manner to both 5' – Deoxyadenosine and 5' – MTA in such experiments (Henshaw et al., [Unpublished manuscript, in progress]).

Chemotactic responses to phage-infected *Synechococcus* at 3 HPI were more variable than responses to cells collected at 7 HPI which may have resulted from variability in the infection timing across experimental replicates. Viruses exhibit temporal control over gene expression (119,120) to optimize their replication cycle. Tight control over timing of gene expression could potentially contribute to the variance observed in chemotactic responses of *V. alginolyticus* if specific exudate concentrations influenced by infection had not yet been manipulated by S-SSM5 to a relevant degree. Phage-infection has been shown to modify host metabolite composition on time scales of minutes (121). The highly productive nature of the infections carried out here (93% of cells remaining at 3 HPI, 59% at 7 HPI, and 24% at 25 HPI) is suggestive of potential differences in *Synechococcus* metabolic exudate profile at 7 HPI as compared to 3 HPI. Nonetheless, *V. alginolyticus* were attracted to intact phage-infected cells to a greater degree as compared to uninfected cells at both 3 and 7 HPI. Interactions between phytoplankton and heterotrophic microbes in the marine environment are important processes that govern the flow of carbon between inorganic and organic states. Modification of carbon flux due to changes in microbial interactions as a result of phage-infection is important for understanding the full spectrum of factors that can influence oceanic biogeochemical cycling. Ultimately, this can lead to the development of predictive models that more accurately incorporate phage influences on nutrient cycling.

Previous studies have quantified bacterial chemotaxis to phytoplankton, their exudates, and lysis products (52,62,86). However, as of this study, no published data are available quantifying bacterial chemotaxis to phage-infected cyanobacteria. Interestingly, direct exchange of metabolites between *Synechococcus* and a chemotactic bacterium, *M.*

adhaerens, at environmentally relevant concentrations was recently quantified (66). This presents evidence contrary to previously held assumptions that *Synechococcus* could not generate a large or dense enough phycosphere to elicit chemotactic responses (87,107) and lends support to the results presented here.

Marine viruses are highly abundant across oceans and exert considerable impact on microbial populations. The results of this study present new data which suggest that marine viruses not only impact the hosts they infect, but can also influence how different species interact during infection which may have implications on a broader scale with respect to nutrient flux in the marine environment. A more comprehensive understanding of how marine viruses manipulate their hosts and microbial interactions is important to developing a more complete picture of the drivers behind the biological carbon pump and other critical processes that govern nutrient and carbon flux in the marine environment.

CONCLUSIONS AND FUTURE DIRECTIONS

Chemotaxis-dependent direct nutrient exchange between *Synechococcus* and a marine bacterium was recently quantified (66), but until this discovery this interaction was generally considered unlikely (87,107). In this study, we assessed the chemotaxis of two marine heterotrophic bacteria, *V. alginolyticus* and *P. haloplanktis*, in response to *Synechococcus* exudates collected from phage-infected cultures and intact phage-infected cells. We observed differential chemotactic responses to phage-infected, as compared to uninfected, treatments for both exudate samples and intact cells that were statistically different, in both cases, at later stages of infection. As of this writing, chemotaxis in response to phage-infected phytoplankton has not been reported in the literature. The data presented in this study, in conjunction with recent quantification of nutrient exchange between *Synechococcus* and chemotactic bacteria (66), shed new light on the role of marine viruses in manipulating chemotaxis which is an important navigational mechanism that influences nutrient exchange. Viral influences on nutrient flux dynamics could have large implications for how we understand carbon cycling especially when considering total viral abundance and estimates of their impact on microbial communities (10,13). A more comprehensive understanding of factors that influence oceanic carbon cycling is important when we consider that: half of all primary production occurs in the oceans and is primarily microbial driven; and increasing temperatures due to global warming are expected to impact the functions and roles of those critical primary producers. To inform future legislation, remediation, and protection efforts, we must understand as much about today's drivers and influencers of carbon cycling to more accurately model system level changes in response to perturbations.

Follow-up experiments to expand on this study could include the measurement and comparison of metabolic exudation rates (115,122,123) in uninfected and phage-infected *Synechococcus* to hone in on the underlying phage-induced changes in hosts that influence differences in chemotactic response. Quantitative MS could provide further insight into whether exudation rate, metabolite concentration, or a combination of factors drive the observed differences in chemotaxis. Experiments evaluating bacterial chemotaxis to specific metabolites, such as those identified in the MS analysis of *Synechococcus* exudates (Figure 11), would provide direct evidence of chemical determinants directly affecting chemotaxis. Another interesting set of experiments would be to assess chemotactic responses of predatory protists to *Synechococcus* exudates under phage-infected conditions. These experiments would investigate the effect of phages on upward trophic transfer of nutrients and would start to link in multiple food web components that may be more representative of an ecological context. Finally, it would be very interesting to compare single cell metrics of chemotaxis in uninfected and phage-infected conditions such as swimming speed, reversal and turning frequencies, residence time within the phycosphere, and encounter rate with *Synechococcus*. Greater temporal (≥ 30FPS) and physical resolution (> 10x magnification) would be important for making accurate measurements. Single cell chemotaxis data would provide depth to our understanding of microbial interactions in response to viral-infection that bulk population measurements (such as those collected in this study) simply cannot.

REFERENCES

1. Field CB, Behrenfeld MJ, Randerson JT, Falkowski P. Primary Production of the Biosphere: Integrating Terrestrial and Oceanic Components. Science. 1998 Jul 10;281(5374):237–40.

2. Falkowski PG, Barber RT, Smetacek V. Biogeochemical Controls and Feedbacks on Ocean Primary Production. Science. 1998 Jul 10;281(5374):200–6.

3. Bar-On YM, Milo R. The Biomass Composition of the Oceans: A Blueprint of Our Blue Planet. Cell. 2019 Dec 12;179(7):1451–4.

4. Flombaum P, Gallegos JL, Gordillo RA, Rincón J, Zabala LL, Jiao N, et al. Present and future global distributions of the marine Cyanobacteria Prochlorococcus and Synechococcus. Proc Natl Acad Sci. 2013 Jun 11;110(24):9824–9.

5. Guidi L, Chaffron S, Bittner L, Eveillard D, Larhlimi A, Roux S, et al. Plankton networks driving carbon export in the oligotrophic ocean. Nature. 2016 Apr;532(7600):465–70.

6. Roxy MK, Modi A, Murtugudde R, Valsala V, Panickal S, Prasanna Kumar S, et al. A reduction in marine primary productivity driven by rapid warming over the tropical Indian Ocean. Geophys Res Lett. 2016;43(2):826–33.

7. Fu W, Randerson JT, Moore JK. Climate change impacts on net primary production (NPP) and export production (EP) regulated by increasing stratification and phytoplankton community structure in the CMIP5 models. Biogeosciences. 2016 Sep 16;13(18):5151–70.

8. Karsenti E, Acinas SG, Bork P, Bowler C, Vargas CD, Raes J, et al. A Holistic Approach to Marine Eco-Systems Biology. PLOS Biol. 2011 Oct 18;9(10):e1001177.

9. Buesseler KO, Boyd PW, Black EE, Siegel DA. Metrics that matter for assessing the ocean biological carbon pump. Proc Natl Acad Sci. 2020 May 5;117(18):9679–87.

10. Suttle CA. Viruses in the sea. Nature. 2005 Sep;437(7057):356–61.

11. Hellebust JA. Excretion of Some Organic Compounds by Marine Phytoplankton. Limnol Oceanogr. 1965;10(2):192–206.

12. Kieft B, Li Z, Bryson S, Hettich RL, Pan C, Mayali X, et al. Phytoplankton exudates and lysates support distinct microbial consortia with specialized metabolic and ecophysiological traits. Proc Natl Acad Sci. 2021 Oct 12;118(41):e2101178118.

13. Suttle CA. Marine viruses — major players in the global ecosystem. Nat Rev Microbiol. 2007 Oct;5(10):801–12.

14. Wilhelm SW, Suttle CA. Viruses and Nutrient Cycles in the Sea | BioScience | Oxford Academic. BioScience. 1999 Oct;49(10):781–8.

15. Proctor LM, Fuhrman JA. Roles of viral infection in organic particle flux. Mar Ecol Prog Ser. 1991;69(1/2):133–42.

16. Middelboe M, Riemann L, Steward GF, Hansen V, Nybroe O. Virus-induced transfer of organic carbon between marine bacteria in a model community. Aquat Microb Ecol. 2003 Aug 21;33(1):1–10.

17. Middelboe M, Jørgensen NOG. Viral lysis of bacteria: an important source of dissolved amino acids and cell wall compounds. J Mar Biol Assoc U K. 2006 Jun;86(3):605–12.

18. Middelboe M, Jorgensen N, Kroer N. Effects of viruses on nutrient turnover and growth efficiency of noninfected marine bacterioplankton. Appl Environ Microbiol. 1996 Jun 1;62(6):1991–7.

19. Weitz JS, Stock CA, Wilhelm SW, Bourouiba L, Coleman ML, Buchan A, et al. A multitrophic model to quantify the effects of marine viruses on microbial food webs and ecosystem processes. ISME J. 2015 Jun;9(6):1352–64.

20. Talmy D, Beckett SJ, Taniguchi DAA, Brussaard CPD, Weitz JS, Follows MJ. An empirical model of carbon flow through marine viruses and microzooplankton grazers. Environ Microbiol. 2019;21(6):2171–81.

21. Lawrence JE, Suttle CA. Effect of viral infection on sinking rates of Heterosigma akashiwo and its implications for bloom termination. Aquat Microb Ecol. 2004 Nov 2;37(1):1–7.

22. Sheyn U, Rosenwasser S, Lehahn Y, Barak-Gavish N, Rotkopf R, Bidle KD, et al. Expression profiling of host and virus during a coccolithophore bloom provides insights into the role of viral infection in promoting carbon export. ISME J. 2018 Mar;12(3):704–13.

23. Jover LF, Effler TC, Buchan A, Wilhelm SW, Weitz JS. The elemental composition of virus particles: implications for marine biogeochemical cycles. Nat Rev Microbiol. 2014 Jul;12(7):519–28.

24. Laber CP, Hunter JE, Carvalho F, Collins JR, Hunter EJ, Schieler BM, et al. Coccolithovirus facilitation of carbon export in the North Atlantic. Nat Microbiol. 2018 May;3(5):537–47.

25. Nissimov JI, Vandzura R, Johns CT, Natale F, Haramaty L, Bidle KD. Dynamics of transparent exopolymer particle production and aggregation during viral infection of the coccolithophore, Emiliania huxleyi. Environ Microbiol. 2018;20(8):2880–97.

26. Yamada Y, Tomaru Y, Fukuda H, Nagata T. Aggregate Formation During the Viral Lysis of a Marine Diatom. Front Mar Sci. 2018;5:167.

27. Evans C, Wilson WH. Preferential grazing of Oxyrrhis marina on virus infected Emiliania huxleyi. Limnol Oceanogr. 2008;53(5):2035–40.

28. Frada MJ, Schatz D, Farstey V, Ossolinski JE, Sabanay H, Ben-Dor S, et al. Zooplankton May Serve as Transmission Vectors for Viruses Infecting Algal Blooms in the Ocean. Curr Biol. 2014 Nov 3;24(21):2592–7.

29. Doherty SC, Maas AE, Steinberg DK, Popp BN, Close HG. Distinguishing zooplankton fecal pellets as a component of the biological pump using compound-specific isotope analysis of amino acids. Limnol Oceanogr. 2021;66(7):2827–41.

30. Zhang C, Dang H, Azam F, Benner R, Legendre L, Passow U, et al. Evolving paradigms in biological carbon cycling in the ocean. Natl Sci Rev. 2018 Jul 1;5(4):481–99.

31. Gobler CJ, Hutchins DA, Fisher NS, Cosper EM, Saňudo-Wilhelmy SA. Release and bioavailability of C, N, P Se, and Fe following viral lysis of a marine chrysophyte. Limnol Oceanogr. 1997;42(7):1492–504.

32. Evans C, Kadner SV, Darroch LJ, Wilson WH, Liss PS, Malin G. The relative significance of viral lysis and microzooplankton grazing as pathways of dimethylsulfoniopropionate (DMSP) cleavage: An Emiliania huxleyi culture study. Limnol Oceanogr. 2007;52(3):1036–45.

33. Hill RW, White BA, Cottrell MT, Dacey JWH. Virus-mediated total release of dimethylsulfoniopropionate from marine phytoplankton: a potential climate process. Aquat Microb Ecol. 1998 Jan 2;14(1):1–6.

34. Malin G, Wilson WH, Bratbak G, Liss PS, Mann NH. Elevated production of dimethylsulfide resulting from viral infection of cultures of Phaeocystis pouchetii. Limnol Oceanogr. 1998;43(6):1389–93.

35. Azam F, Fenchel T, Field JG, Gray JS, Meyer-Reil LA, Thingstad F. The Ecological Role of Water-Column Microbes in the Sea. Mar Ecol Prog Ser. 1983;10(3):257–63.

36. Falkowski PG. Photosynthesis: The paradox of carbon dioxide efflux. Curr Biol. 1997 Oct 1;7(10):R637–9.

37. Wilson WH, Joint IR, Carr NG, Mann NH. Isolation and Molecular Characterization of Five Marine Cyanophages Propagated on Synechococcus sp. Strain WH7803. Appl Environ Microbiol. 1993 Nov 1;59(11):3736–43.

38. Waterbury JB, Valois FW. Resistance to Co-Occurring Phages Enables Marine Synechococcus Communities To Coexist with Cyanophages Abundant in Seawater. Appl Environ Microbiol. 1993 Oct 1;59(10):3393–9.

39. Suttle CA, Chan AM. Marine cyanophages infecting oceanic and coastal strains of Synechococcus: abundance, morphology, cross-infectivity and growth characteristics. Mar Ecol Prog Ser. 1993;92(1/2):99–109.

40. Clokie MR, Millard AD, Mann NH. T4 genes in the marine ecosystem: studies of the T4-like cyanophages and their role in marine ecology. Virol J. 2010 Oct 28;7(1):291.

41. Yap ML, Rossmann MG. Structure and function of bacteriophage T4. Future Microbiol. 2014 Oct;9:1319–27.

42. Xu X, Khudyakov I, Wolk CP. Lipopolysaccharide dependence of cyanophage sensitivity and aerobic nitrogen fixation in Anabaena sp. strain PCC 7120. J Bacteriol. 1997 May 1;179(9):2884–91.

43. Mann NH, Cook A, Millard A, Bailey S, Clokie M. Bacterial photosynthesis genes in a virus. Nature. 2003 Aug;424(6950):741–741.

44. Sullivan MB, Lindell D, Lee JA, Thompson LR, Bielawski JP, Chisholm SW. Prevalence and Evolution of Core Photosystem II Genes in Marine Cyanobacterial Viruses and Their Hosts. PLOS Biol. 2006 Jul 4;4(8):e234.

45. Millard A, Clokie MRJ, Shub DA, Mann NH. Genetic organization of the psbAD region in phages infecting marine Synechococcus strains. Proc Natl Acad Sci. 2004 Jul 27;101(30):11007–12.

46. Howard-Varona C, Roux S, Bowen BP, Silva LP, Lau R, Schwenck SM, et al. Protist impacts on marine cyanovirocell metabolism. ISME Commun. 2022 Oct 1;2(1):1–14.

47. Luchsinger RH, Bergersen B, Mitchell JG. Bacterial Swimming Strategies and Turbulence. Biophys J. 1999 Nov 1;77(5):2377–86.

48. Hill NA, Häder DP. A Biased Random Walk Model for the Trajectories of Swimming Micro-organisms. J Theor Biol. 1997 Jun 21;186(4):503–26.

49. Alt W. Biased random walk models for chemotaxis and related diffusion approximations. J Math Biol. 1980 Apr 1;9(2):147–77.

50. Kawagishi I, Maekawa Y, Atsumi T, Homma M, Imae Y. Isolation of the polar and lateral flagellum-defective mutants in Vibrio alginolyticus and identification of their flagellar driving energy sources. J Bacteriol. 1995 Sep;177(17):5158–60.

51. Xie L, Altindal T, Chattopadhyay S, Wu XL. Bacterial flagellum as a propeller and as a rudder for efficient chemotaxis. Proc Natl Acad Sci. 2011 Feb 8;108(6):2246–51.

52. Barbara GM, Mitchell JG. Bacterial tracking of motile algae. FEMS Microbiol Ecol. 2003 May;44(1):79–87.

53. Locsei JT, Pedley TJ. Bacterial Tracking of Motile Algae Assisted by Algal Cell's Vorticity Field. Microb Ecol. 2009 Jul 1;58(1):63–74.

54. Mitchell JG, Pearson L, Bonazinga A, Dillon S, Khouri H, Paxinos R. Long lag times and high velocities in the motility of natural assemblages of marine bacteria. Appl Environ Microbiol. 1995 Mar;61(3):877–82.

55. Magariyama Y, Sugiyama S, Muramoto K, Maekawa Y, Kawagishi I, Imae Y, et al. Very fast flagellar rotation. Nature. 1994 Oct;371(6500):752–752.

56. Berg HC. The Rotary Motor of Bacterial Flagella. Annu Rev Biochem. 2003;72(1):19–54.

57. Fenchel T. The microbial loop – 25 years later. J Exp Mar Biol Ecol. 2008 Nov;366(1–2):99–103.

58. Golding I, Paulsson J, Zawilski SM, Cox EC. Real-Time Kinetics of Gene Activity in Individual Bacteria. Cell. 2005 Dec 16;123(6):1025–36.

59. Olson ER. Influence of pH on bacterial gene expression. Mol Microbiol. 1993;8(1):5–14.

60. Winkler WC, Breaker RR. Regulation of Bacterial Gene Expression by Riboswitches. Annu Rev Microbiol. 2005;59(1):487–517.

61. Hurwitz BL, Hallam SJ, Sullivan MB. Metabolic reprogramming by viruses in the sunlit and dark ocean. Genome Biol. 2013 Nov 7;14(11):R123.

62. Smriga S, Fernandez VI, Mitchell JG, Stocker R. Chemotaxis toward phytoplankton drives organic matter partitioning among marine bacteria. Proc Natl Acad Sci. 2016 Feb 9;113(6):1576–81.

63. Stocker R, Seymour JR, Samadani A, Hunt DE, Polz MF. Rapid chemotactic response enables marine bacteria to exploit ephemeral microscale nutrient patches. Proc Natl Acad Sci. 2008 Mar 18;105(11):4209–14.

64. Seymour JR, Marcos, Stocker R. Resource Patch Formation and Exploitation throughout the Marine Microbial Food Web. Am Nat. 2009 Jan 1;173(1):E15–29.

65. Seymour JR, Ahmed T, Durham WM, Stocker R. Chemotactic response of marine bacteria to the extracellular products of Synechococcus and Prochlorococcus. Aquat Microb Ecol. 2010 Mar 31;59(2):161–8.

66. Raina JB, Giardina M, Brumley DR, Clode PL, Pernice M, Guagliardo P, et al. Chemotaxis increases metabolic exchanges between marine picophytoplankton and heterotrophic bacteria. Nat Microbiol. 2023 Mar;8(3):510–21.

67. Harrison PJ, Waters RE, Taylor FJR. A BROAD SPECTRUM ARTIFICIAL SEA WATER MEDIUM FOR COASTAL AND OPEN OCEAN PHYTOPLANKTON [1]. J Phycol. 1980 Mar;16(1):28–35.

68. Berges JA, Franklin DJ, Harrison PJ. Evolution of an Artificial Seawater Medium: Improvements in Enriched Seawater, Artificial Water Over the Last Two Decades. J Phycol. 2001;37(6):1138–45.

69. Xia Y, Whitesides GM. Soft Lithography. Annu Rev Mater Sci. 1998;28(1):153–84.

70. Dufresne E, Blair D, Grier D, Crocker J, Weeks E. Matlab Particle Tracking (bpass, pkfnd, cntrd) [Internet]. 1997 [cited 2023 Apr 1]. Available from: https://site.physics.georgetown.edu/matlab/index.html

71. Aron AT, Gentry EC, McPhail KL, Nothias LF, Nothias-Esposito M, Bouslimani A, et al. Reproducible molecular networking of untargeted mass spectrometry data using GNPS. Nat Protoc. 2020 Jun;15(6):1954–91.

72. Shannon P, Markiel A, Ozier O, Baliga NS, Wang JT, Ramage D, et al. Cytoscape: a software environment for integrated models of biomolecular interaction networks. Genome Res. 2003 Nov;13(11):2498–504.

73. Homma M, Oota H, Kojima S, Kawagishi I, Imae Y 1996. Chemotactic responses to an attractant and a repellent by the polar and lateral flagellar systems of Vibrio alginolyticus. Microbiology. 142(10):2777–83.

74. Stehnach MR, Henshaw RJ, Floge SA, Guasto JS. Multiplexed microfluidic screening of bacterial chemotaxis [Internet]. Ecology; 2022 Dec [cited 2023 Jan 31]. Available from: http://biorxiv.org/lookup/doi/10.1101/2022.11.30.518228

75. Son K, Menolascina F, Stocker R. Speed-dependent chemotactic precision in marine bacteria. Proc Natl Acad Sci. 2016 Aug 2;113(31):8624–9.

76. Yamashita M, Fenn JB. Electrospray ion source. Another variation on the free-jet theme [Internet]. ACS Publications. American Chemical Society; 2002 [cited 2023 Feb 17]. Available from: https://pubs.acs.org/doi/pdf/10.1021/j150664a002

77. Wilm M. Principles of Electrospray Ionization. Mol Cell Proteomics [Internet]. 2011 Jul 1 [cited 2023 Feb 17];10(7). Available from: https://www.mcponline.org/article/S1535-9476(20)30199-7/abstract

78. Barbara GM, Mitchell JG. Marine bacterial organisation around point-like sources of amino acids. FEMS Microbiol Ecol. 2003 Feb 1;43(1):99–109.

79. Weinstock MT, Hesek ED, Wilson CM, Gibson DG. Vibrio natriegens as a fast-growing host for molecular biology. Nat Methods. 2016 Oct;13(10):849–51.

80. Sandle T. Disinfectants. In: Rezaei N, editor. Encyclopedia of Infection and Immunity [Internet]. Oxford: Elsevier; 2022 [cited 2023 Jan 18]. p. 630–9. Available from: https://www.sciencedirect.com/science/article/pii/B9780128187319002068

81. Johnson WM, Soule MCK, Longnecker K, Bhatia MP, Hallam SJ, Lomas MW, et al. Insights into the controls on metabolite distributions along a latitudinal transect of the western Atlantic Ocean [Internet]. bioRxiv; 2021 [cited 2022 Sep 12]. p. 2021.03.09.434501. Available from: https://www.biorxiv.org/content/10.1101/2021.03.09.434501v1

82. Segall JE, Block SM, Berg HC. Temporal comparisons in bacterial chemotaxis. Proc Natl Acad Sci. 1986 Dec;83(23):8987–91.

83. Clark DA, Grant LC. The bacterial chemotactic response reflects a compromise between transient and steady-state behavior. Proc Natl Acad Sci. 2005 Jun 28;102(26):9150–5.

84. Tu Y, Shimizu TS, Berg HC. Modeling the chemotactic response of Escherichia coli to time-varying stimuli. Proc Natl Acad Sci. 2008 Sep 30;105(39):14855–60.

85. Seymour JR, Simó R, Ahmed T, Stocker R. Chemoattraction to Dimethylsulfoniopropionate Throughout the Marine Microbial Food Web. Science. 2010 Jul 16;329(5989):342–5.

86. Seymour JR, Ahmed T, Stocker R. Bacterial chemotaxis towards the extracellular products of the toxic phytoplankton Heterosigma akashiwo. J Plankton Res. 2009 Dec 1;31(12):1557–61.

87. Stocker R, Seymour JR. Ecology and Physics of Bacterial Chemotaxis in the Ocean. Microbiol Mol Biol Rev. 2012 Dec 1;76(4):792–812.

88. Raina JB, Fernandez V, Lambert B, Stocker R, Seymour JR. The role of microbial motility and chemotaxis in symbiosis. Nat Rev Microbiol. 2019 May;17(5):284–94.

89. Mesibov R, Adler J. Chemotaxis Toward Amino Acids in Escherichia coli. J Bacteriol. 1972 Oct;112(1):315–26.

90. Blackburn N, Fenchel T, Mitchell J. Microscale Nutrient Patches in Planktonic Habitats Shown by Chemotactic Bacteria. Science. 1998 Dec 18;282:2254–6.

91. Salek MM, Carrara F, Fernandez V, Guasto JS, Stocker R. Bacterial chemotaxis in a microfluidic T-maze reveals strong phenotypic heterogeneity in chemotactic sensitivity. Nat Commun. 2019 Apr 23;10(1):1877.

92. de Gennes PG. Chemotaxis: the role of internal delays. Eur Biophys J. 2004 Dec 1;33(8):691–3.

93. Ortmann AC, Suttle CA. High abundances of viruses in a deep-sea hydrothermal vent system indicates viral mediated microbial mortality. Deep Sea Res Part Oceanogr Res Pap. 2005 Aug;52(8):1515–27.

94. Guixa-Boixereu N, Vaqué D, Gasol JM, Sánchez-Cámara J, Pedrós-Alió C. Viral distribution and activity in Antarctic waters. Deep Sea Res Part II Top Stud Oceanogr. 2002 Jan 1;49(4):827–45.

95. Suttle CA. The significance of viruses to mortality in aquatic microbial communities. Microb Ecol. 1994 Sep 1;28(2):237–43.

96. Zimmerman AE, Howard-Varona C, Needham DM, John SG, Worden AZ, Sullivan MB, et al. Metabolic and biogeochemical consequences of viral infection in aquatic ecosystems. Nat Rev Microbiol. 2020 Jan;18(1):21–34.

97. Turner JT. Zooplankton fecal pellets, marine snow, phytodetritus and the ocean's biological pump. Prog Oceanogr. 2015 Jan 1;130:205–48.

98. Hansell DA, Carlson CA, Repeta DJ, Schlitzer R. Dissolved Organic Matter in the Ocean: A Controversy Stimulates New Insights. Oceanography. 2009;22(4):202–11.

99. Pontiller B, Martínez-García S, Lundin D, Pinhassi J. Labile Dissolved Organic Matter Compound Characteristics Select for Divergence in Marine Bacterial Activity and Transcription. Front Microbiol [Internet]. 2020 [cited 2023 Feb 9];11. Available from: https://www.frontiersin.org/articles/10.3389/fmicb.2020.588778

100. Lønborg C, Middelboe M, Brussaard CPD. Viral lysis of Micromonas pusilla: impacts on dissolved organic matter production and composition. Biogeochemistry. 2013 Dec 1;116(1):231–40.

101. Fouilland E, Tolosa I, Bonnet D, Bouvier C, Bouvier T, Bouvy M, et al. Bacterial carbon dependence on freshly produced phytoplankton exudates under different nutrient availability and grazing pressure conditions in coastal marine waters. FEMS Microbiol Ecol. 2014 Mar;87(3):757–69.

102. Kiørboe T, Jackson GA. Marine snow, organic solute plumes, and optimal chemosensory behavior of bacteria. Limnol Oceanogr. 2001;46(6):1309–18.

103. Kiørboe T, Grossart HP, Ploug H, Tang K. Mechanisms and Rates of Bacterial Colonization of Sinking Aggregates. Appl Environ Microbiol. 2002 Aug;68(8):3996–4006.

104. Honjo S, Manganini SJ, Krishfield RA, Francois R. Particulate organic carbon fluxes to the ocean interior and factors controlling the biological pump: A synthesis

of global sediment trap programs since 1983. Prog Oceanogr. 2008 Mar;76(3):217–85.

105. Evans C, Pond D, Wilson W. Changes in Emiliania huxleyi fatty acid profiles during infection with E. huxleyi virus 86: physiological and ecological implications. Aquat Microb Ecol. 2009 May 8;55(3):219–28.

106. Mitchell JG, Okubo A, Fuhrman JA. Microzones surrounding phytoplankton form the basis for a stratified marine microbial ecosystem. Nature. 1985 Jul;316(6023):58–9.

107. Seymour JR, Amin SA, Raina JB, Stocker R. Zooming in on the phycosphere: the ecological interface for phytoplankton–bacteria relationships. Nat Microbiol. 2017 May 30;2(7):1–12.

108. Biddanda B, Benner R. Carbon, nitrogen, and carbohydrate fluxes during the production of particulate and dissolved organic matter by marine phytoplankton. Limnol Oceanogr. 1997;42(3):506–18.

109. Sheik AR, Brussaard CPD, Lavik G, Lam P, Musat N, Krupke A, et al. Responses of the coastal bacterial community to viral infection of the algae Phaeocystis globosa. ISME J. 2014 Jan;8(1):212–25.

110. Bjørrisen PK. Phytoplankton exudation of organic matter: Why do healthy cells do it?1. Limnol Oceanogr. 1988;33(1):151–4.

111. Thornton DCO. Dissolved organic matter (DOM) release by phytoplankton in the contemporary and future ocean. Eur J Phycol. 2014 Jan 2;49(1):20–46.

112. Bell W, Mitchell R. CHEMOTACTIC AND GROWTH RESPONSES OF MARINE BACTERIA TO ALGAL EXTRACELLULAR PRODUCTS. Biol Bull. 1972 Oct;143(2):265–77.

113. Brussaard CPD. Optimization of Procedures for Counting Viruses by Flow Cytometry. Appl Environ Microbiol. 2004 Mar 1;70(3):1506–13.

114. Brussaard CPD, Payet JP, Winter C, Weinbauer MG. Quantification of aquatic viruses by flow cytometry. In: Wilhelm S, Weinbauer M, Suttle C, editors. Manual of Aquatic Viral Ecology [Internet]. American Society of Limnology and Oceanography; 2010 [cited 2023 Apr 19]. p. 102–9. Available from: http://www.aslo.org/books/mave/102.html

115. Bowen JD, Stolzenbach KD, Chisholm SW. Simulating bacterial clustering around phytoplankton cells in a turbulent ocean. Limnol Oceanogr. 1993;38(1):36–51.

116. Aaronson S. Excretion of organic matter by phytoplankton in vitro. Limnol Oceanogr. 1978;23(4):838–838.

117. Fogg GE. Excretion of organic matter by phytoplankton. Limnol Oceanogr. 1977;22(3):576–7.

118. Jones AK, Cannon RC. The release of micro-algal photosynthate and associated bacterial uptake and heterotrophic growth. Br Phycol J. 1986 Dec 1;21(4):341–58.

119. James TD, Cashel M, Hinton DM. A Mutation within the β Subunit of Escherichia coli RNA Polymerase Impairs Transcription from Bacteriophage T4 Middle Promoters. J Bacteriol. 2010 Nov;192(21):5580–7.

120. Miller ES, Kutter E, Mosig G, Arisaka F, Kunisawa T, Rüger W. Bacteriophage T4 Genome. Microbiol Mol Biol Rev. 2003 Mar;67(1):86–156.

121. De Smet J, Zimmermann M, Kogadeeva M, Ceyssens PJ, Vermaelen W, Blasdel B, et al. High coverage metabolomics analysis reveals phage-specific alterations to Pseudomonas aeruginosa physiology during infection. ISME J. 2016 Aug;10(8):1823–35.

122. Baines SB, Pace ML. The production of dissolved organic matter by phytoplankton and its importance to bacteria: Patterns across marine and freshwater systems. Limnol Oceanogr. 1991 Sep;36(6):1078–90.

123. Wolter K. Bacterial Incorporation of Organic Substances Released by Natural Phytoplankton Populations. Mar Ecol Prog Ser. 1982;7(3):287–95.

CURRICULUM VITAE

Jonathan Moon

moonjd21@wfu.edu

Education

May 2023 **M.S. Biology**, Wake Forest University, Winston-Salem, NC, USA
Thesis: "Marine Heterotrophic Bacterial Chemotaxis to Phage-Infected *Synechococcus*"
Advisor: Sheri Floge, Ph.D.

Dec 2016 **B.S. Biology**, Towson University, Towson, MD, USA

Publications

Henshaw, Richard[1,2]; **Moon, Jonathan**[3]; Floge, Sheri[3]; Guasto, Jeffrey[1]. (2023) Early Viral Infection of Cyanobacteria Drives Bacterial Chemotaxis in the Oceans. [Unpublished Manuscript, in progress].[1]Department of Mechanical Engineering, Tufts University, [2]Institute of Environmental Engineering, ETH Zurich, [3]Department of Biology, Wake Forest University

Moon, J. and E.M. Barry. Sequence Variations in the ETEC CS6 Operon Affect Transcript and Protein Expression. *Virulence*, 2021, Dec; 12(1):2659-2669. PMC8923064

Pilla, G.; Wu, T.; Grassel, C.; **Moon, J.**; Foulke-Abel, J.; Tang, C.M.; Barry, E.M. Evaluation of a Live Attenuated *S. sonnei* Vaccine Strain in the Human Enteroid Model. *Pathogens* 2021, *10*, 1079. https://doi.org/10.3390/pathogens10091079

Research

Aug 2021 – May 2023 **Graduate Student**, Biology, Wake Forest University
Research Advisor: Sheri Floge, Ph.D.
Description:
Quantification of marine heterotrophic bacterial chemotaxis in response to phage-infected cyanobacteria

June 2017 – July 2021 **Research Specialist**, Center for Vaccine Development and Global Health, University of Maryland, Baltimore
Research Advisor: Eileen Barry, Ph.D.
Description:
Engineering and development of a live-attenuated multivalent vaccine targeting *S. flexneri* and ETEC

Grants and Awards

October 2021 **Vecellio Grants for Graduate Research** (WFU)